MASTER COPY KEEP FOR REPRODUCTION PURPOSES

REPORT DOCUMENTATION PAGE

Form Approved
OMB NO. 0704-0188

1. AGENCY USE ONLY *(Leave blank)*	2. REPORT DATE	3. REPORT TYPE AND DATES COVERED
	April 23, 1999	Final Report 02/21/97-02/21/99

4. TITLE AND SUBTITLE
Small, Efficient Thermophotovoltaic Power Supply

5. FUNDING NUMBERS
DAAG55-97-C-0003

6. AUTHOR(S)
Dr. K. C. Chen, Mr. Dale Osborn and Mr. Pedro A. Sarmiento (Quantum)
Mr. Sunil Earath, Dr. A. J. Prasad (University of Delaware)

7. PERFORMING ORGANIZATION NAMES(S) AND ADDRESS(ES)
Quantum Group, Inc.
11211 Sorrento Valley Road
San Diego, CA 92121

8. PERFORMING ORGANIZATION REPORT NUMBER
QGI-0010

9. SPONSORING / MONITORING AGENCY NAME(S) AND ADDRESS(ES)
U.S. Army Research Office
P.O. Box 12211
Research Triangle Park,, NC 27709-2211

10. SPONSORING / MONITORING AGENCY REPORT NUMBER
ARO 36332.1-RT-ST2

11. SUPPLEMENTARY NOTES
The views, opinions and/or findings contained in this report are those of the author(s) and should not be construed as an official Department of the Army position, policy or decision, unless so designated by other documentation.

12a. DISTRIBUTION / AVAILABILITY STATEMENT
Approved for public release; distribution unlimited.

12 b. DISTRIBUTION CODE

13. ABSTRACT *(Maximum 200 words)*

The objective of this contract is to design and build a small, lightweight, stand-alone thermophotovoltaic electric generator, capable of at least 100 Watts useful output for charging 24V batteries.

The prototype generator built consists of a pre-mixed burner, a cylindrical selective emitter mantle surrounded by six silicon photovoltaic concentrator arrays. The arrays are cooled with forced-air heat exchangers using self-powered fans. The generator, operated at 11700 W (40,000 BTU/hr) of fuel input rate, produces 122W of electrical power at 1.0% of efficiency. The cooling and pre-mix fans consume 35W of electrical power resulting in a net 85 Watts of electrical output for charging batteries. The generator's output is capable of continuous charging five 12/24V batteries over 10 hours with a 9.07 Kg (20 lbs.) of propane gas.

14. SUBJECT TERMS	15. NUMBER IF PAGES
thermophotovoltaic, generator, photocell, array, selective emitter, mantle, ytterbia,	46
	16. PRICE CODE

17. SECURITY CLASSIFICATION OR REPORT	18. SECURITY CLASSIFICATION OF THIS PAGE	19. SECURITY CLASSIFICATION OF ABSTRACT	20. LIMITATION OF ABSTRACT
UNCLASSIFIED	UNCLASSIFIED	UNCLASSIFIED	UL

Small, Efficient Thermophotovoltaic Power Supply

Final Technical Report

Dr. K. C. Chen
Mr. Dale Osborn
Mr. Pedro Sarmiento
Quantum Group, Inc. San Diego
and
Dr. Ajay Prasad
Mr. Sunil Earath
Department of Mechanical Engineering,
University of Delaware

21 February 1997 to 21 February 1999

U.S. ARMY RESEARCH OFFICE

Contract Number DAAG55-97-C-0003

Quantum Group, Inc.
11211 Sorrento Valley Road
San Diego, CA 92121

TABLE OF CONTENTS

LIST OF FIGURES

LIST OF TABLE

1. Statement of the Problem Studied

With the heavy use of electronics today, the U.S. Army must provide soldiers with a daily supply of freshly charged batteries to power their equipment. It is estimated that approximately $75 million is currently spent by the U.S. Army on throwaway batteries. The cost of disposal and environmental impact has led the Army Directive to shift to rechargeable batteries in the future. In the short or near term, the goal is to reduce battery associated costs by 50%. To use rechargeable batteries, a reliable and convenient way to recharge the batteries in the field is necessary. Currently, the Army uses sealed nickel metal hydride rechargeable batteries (e.g. BB-390A/U) that are recharged by a 12V/24V battery charger (PP-8444A/U). This research is in response to the Army's need to have a portable electrical power generator to recharge the battery. The objective of Quantum Group, Inc. is to design and build a portable thermophotovoltaic (TPV) generator prototype, capable of at least 100 Watts useful output. The design was oriented toward use of a generator as a 24 Volt battery charger, but other applications are feasible.

2. Program Goal and Summary of the Most Important Results

The generator design goal is to provide at least 100 Watts, 24 VDC power output within an envelope dimension of 37 cm (15 inch) diameter and 45 cm (18 inch) height. The target weight, excluding fuel, is 6.8 Kg (15 lb.). Replacing some aluminum parts with composite material can further reduce the weight. The generator runs on 9.07 Kg (20 lbs.) propane fuel. The system goal is targeted at 5 % efficiency.

Figure 1 shows the prototype TPV generator. The prototype weighs 9.09 Kg (20 lb.) and its dimensions are within the design goal. The prototype generator produces 122 W of electric power at a voltage of 24 V and a current of 5 Amperes. The efficiency is 1% with the fuel input rate of 40,000 BTU/hr (117,00 W). The main shortfall in efficiency is due to a large end radiation loss in the cylindrical geometry. This loss can be improved with the addition of end reflectors and closing the spacing between emitter and PV arrays. The stand-alone unit requires cooling fans. The power requirement for six Micronel® cooling fans plus one fan for pre-mixer is 37 Watts, therefore, the generator produces a net power output of 85 Watts for charging batteries. At the operation fuel rate, a 9.07 Kg propane tank (5 gallon) can run continuously for 10 hours and charge 5 batteries.

The first stage of the program studied and analyzed design approaches and performed parametric studies of key component design. During this period, the heat transfer parameters of the heat exchanger were defined, simulated, optimized and then verified through testing (see **Array Cooling** section). The photovoltaic cell layout and interconnection method were determined. Two PV vendors were evaluated for price and on-time delivery. The difficulties that were come across were the larger-than-the-expected photocell arrays cost and the long lead time for the manufacturing of heat exchanger. Funds had to be re-allocated to acquire seven PV arrays. Bonding the PV arrays to heat sink was assumed by Quantum Group in order to reduce overall cost.

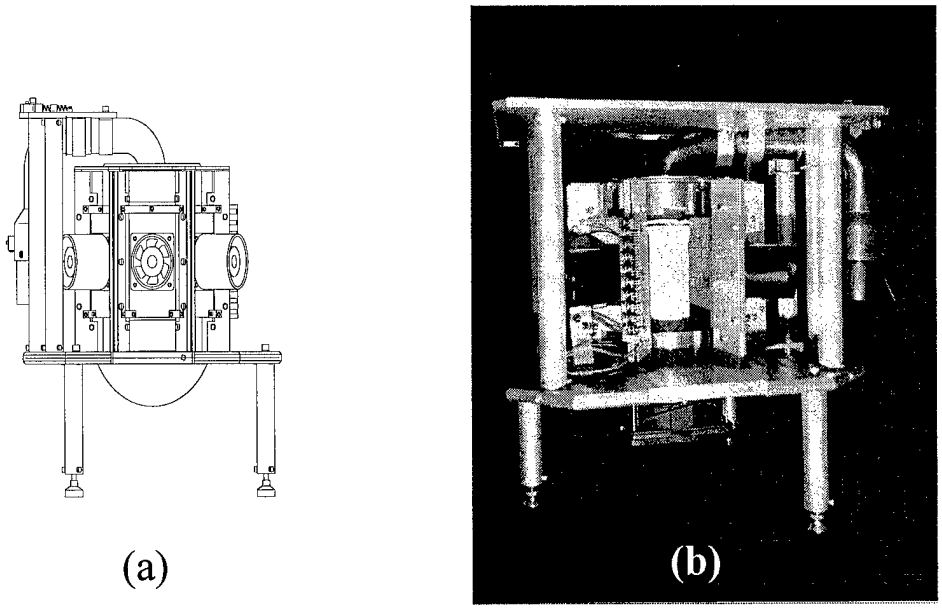

Figure 1. The prototype TPV generator (a) conceptual drawing, and (b) final assembly.

The second portion of the program was a hardware development stage. This stage concentrated on designing a specific configuration of the basic elements, testing and characterization of each element, then integrating these elements into a prototype TPV generator. During this period, the microchannel heat exchangers were fabricated according to the specified fin height of 1.9 cm (0.75 in.), and the specified fin spacing of ~ 7.8 fin/cm (20 fin/in). PV arrays were ordered and successfully bonded to heat exchangers and tested. The performance of the gas train, mantle durability, PV sub-arrays, and PV array output, heat exchanger and ignitor location were evaluated. The generator went through a few design modifications during the development. The L-shaped and U-shaped gas trains were tested for fuel inlet. The original extended tripod design for mantle replacement was changed to a low-profile version for better generator stability.

In conclusion, a prototype TPV generator was successfully fabricated. This unit produces 85 Watts of net electrical power output at 24V. The generator, however, lacks a self-diagnostic feature. It is believed that this feature is needed for automated operation for the soldier. There are also a few remaining packaging and operational issues, including the automatic interlocking solenoid control, before the generator can be field tested.

3. Major Areas of Effort

3.1 Background

A brief description of the basic operation of the TPV generator addressed in this effort and important considerations for the design are given below. A thermophotovoltaic generator

converts chemical energy to electrical energy through thermally generated photons. In practice, energy stored in the fuel is converted to heat through combustion. Heat from the combustion elevates a ceramic mantle to an incandescent temperature and emits photons. Photocells are used to convert the photon energy to electricity. The important generator design consideration is to increase the efficiencies in each energy conversion step.

Generator designs and performance have many tradeoffs. At a high fuel input rate, radiation output drastically increases as the mantle temperature increases. At the same time, however, a higher portion of the heat is lost in the flue gas and more heat needs to be removed from the photovoltaic (PV) cell. There is a limitation on the volume of primary air that can be adequately provided by the fan without incurring substantial back pressure. It was calculated that ytterbia has better efficiency at 2000°C, but in reality, limitations on high temperature material strength and propane flame temperature dictates the upper operation temperature. There is also a less than optimal *view factor* when coupling a cylindrical emitter to a planar PV arrays. This contributes a sizable radiation loss. The PV cell's efficiency decreases with increasing temperature. Maintaining an acceptable PV temperature by using cooling fans drains energy from the system The optimal generator design is, therefore, a compromise between increasing total energy output, system efficiency, and decreasing cooling power consumption. The system weight, compactness, raggedness, and user-friendly operation are also system design criteria.

3..2 Studies and Analyses

3.2.1 Selective emitter

At the heart of the thermophotovoltaic generation process, and one of the keys to its efficiency over a blackbody system, is the mantle material. The generator system uses a selective emitter material made of ytterbia oxide (Yb_2O_3). At high temperature, ytterbia emits a narrow band of photons, with wavelengths centered at 980 nm and a full-width half-maximum (FWHM) of 200 nm, that matches silicon photocell response. Therefore, the silicon-in-band photons can be more efficiently converted to electricity than a blackbody emitter. The radiant flux measurement indicated 58% of the ytterbia emissive energy is within the convertible band of silicon PV cell (see **Figure 6, page 12 of the 1st Quarterly Technical Report, April 1997**).

The mantle provides a surface for combustion. Its weave density affects the power generation and efficiency of the TPV generator. Outputs of mantles made of two weave densities were examined using a single Amonix cell. Mantle emission increases significantly with denser weave (**figure 1 of the Interim Progress Report, Dec. 1997**). The dense-weave Yb_2O_3 mantle has 58% silicon-in-band radiation (i.e. $E_{0.4\text{-}1.1\mu m}/E_{1.1\text{-}14.0\mu m}$) versus a light-weave mantle of 52%. A *double-layered* dense-weave mantle can further increase the radiant output (**Table 1**), and it has the benefit of increasing the *apparent* strength under high velocity fuel. It is, however, more difficult to ignite consistently and was not suitable in generator use.

Mantle output was found to be non-linear with mantle fuel loading; A small increase at low loading, a large increase at moderate loading, and little increase at high loading. When the mantle surface fuel loading increases 2.5 times from 31.5 to 79 W/cm^2 (2970W/1186W), the peak height only increases 1.36-1.46 times. This indicates decreasing mantle radiant efficiency

at high fuel loading (**Interim Progress Report, figures 4, Dec. 1997**). At 40,000 Btu/hr fuel input rate, the generator has a mantle surface fuel loading of 66 W/cm^2, where fuel to silicon-in-band radiation efficiency is measured at 13% (**Figure 2**).

The mantle durability is influenced by the fabrication process and also the geometry of the distributor. If a mantle is not sufficiently converted to hydroxide during the fabrication process,

Table 1. Performance of mantle under different fuel input rates and layers measured in a single Amonix cell.

Fuel Input Rate (W)	Number of Layers	Single Amonix cell Power Output (W)
8,800	Single	0.42
11,700	Single	0.46
14,600	Single	0.54
14,600	Double	0.67

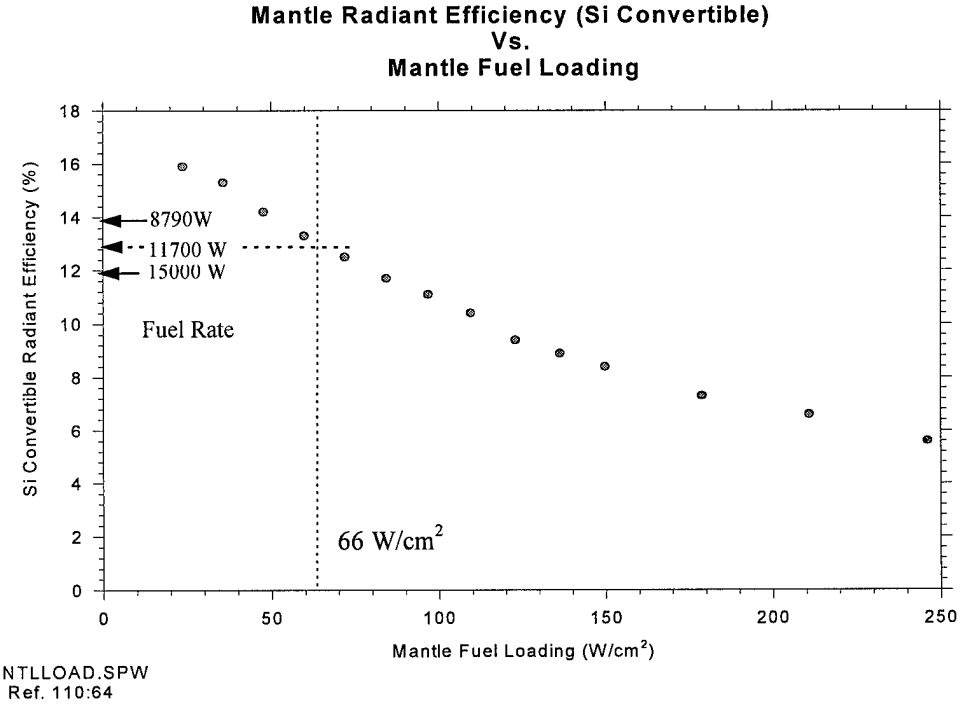

Figure 2. Silicon convertible radiation fraction versus fuel input energy rate normalized by gross mantle area.

the limit of the fuel input rate is around 40,000 Btu/hr. Above this fuel input rate, mantles would often tear under the high pressure and velocity of fuel through the perforated distributor cone. Later, improvement in the mantle fabrication process was made and the mantle was able to run at 50,000 Btu/hr fuel input. The generator is operated at 40,000 Btu/hr—not because of mantle strength limitation but the 100 °C temperature limit at the PV cells. A double-layered mantle is able to run at 50,000 Btu/hr. During the first ignition, however, it generates more smoke and often has an uneven shrinkage. The durability of single- and double-layered mantles was evaluated in tests with continuous operating periods of up to 8-10 hours at 51,000 Btu/hr. No visible damage or reduction in optical output was observed. The continuous operation allows charging a number of batteries with a minimum of operator involvement. It should be noted that the mantle is intended to be used after a single ignition and then continuously operated. Re-ignition after long operation weakens and fractures the mantle. A pre-burnt hard mantle approach has been evaluated. The hard mantle has a supporting structure at mantle's both ends. This should increase the shock and vibration resistance of the mantle, allowing the generator to be run at off-vertical orientation and quick mantle replacement in the field. This option is still viable for future improvement.

The mantle radiant profile along the mantle axis was measured using a Gorden Gauge and SR5000 spectrophotometer. The result was used to model the heat flux on the PV cell (see **Array Cooling** section). This profile also indicated that there is an axial variation in radiant flux along the length of the emitter. Experiments were performed to see if the radiant profile can be made more uniform along the axis of the mantle by using different burner heads.

3.2.2 Reduction of First Ignition Combustion Byproducts

The first ignition of the mantle generates smoke. This smoke could quickly damage the filter, photocell arrays, and blower by a build-up of coke on the surfaces. An effort was made to reduce the amount of smoke generated by changing the mantle preparation process. The mantles were processed in an inert furnace to transform the rayon into a partially graphitic state. With a strong thermal gradient, the upper attachment portion of the mantle did not transform into the graphitic state. It remained to be a flexible rayon. The result is a mantle with the upper portion still normal rayon with a gradual transition into a black graphitic rayon portion. This configuration allows easier mantle attachment without damaging it, and produced much less smoke on first ignition. The drawback is that the graphitic portion burns much slower than the rayon state, so it is better to burn it with the assistance of the fan. With the introduction of fuel and air mixture, the mantle retained an acceptable geometry for generator operation.

3.2.3 Mantle Re-ignition

As the fuel input rate is increased, the mantle temperature increases. If the mantle is operated above 45,000 Btu/hr, it becomes quite fragile during the cool-down process. Upon restarting, the mantle often fractures immediately. One other major factor that decreases the mantle strength was found to be an insufficient de-nitration step in mantle processing. The mantle process has

been standardized to minimize property variation. In any case, the mantle emitter is to be used after a single ignition. However, the mantle is shown to continuously operate more than 10 hours, so this may not be an operational problem.

Ultimately, the mantle's strength and thermal shock resistance can only be improved by hindering secondary grain growth and sintering of the fibers at operational temperatures. It is well known that the strength of ceramic is inversely proportional to the square-root of the grain size. The Orowan relation $\sigma_f = k_2 d^{-1/2}$ predicts that strength decreases with increasing grain size. The thermal shock resistance is also related to the grain size. The relation is represented as $\Delta T_f = \sigma_f \times (1-\mu)/Ea$, where ΔT_f is the temperature difference when the fracture stress level is reached; σ_f is the fracture stress that is related to grain size as stated before, μ is the Poisson's ratio, E is the elastic modules, and a is the thermal expansion coefficient. After high temperature operation, the fiber has a much larger grain size, hence lower mechanical strength. Thermal shock resistance significantly decreases after continuous operation because of the decrease in the fracture stress level.

At low temperature, sintering of one fiber to the next is very limited. The mantle normally remains flexible because fiber tows (strands of small fibers) bend and slide across each other when they are subjected to thermal stress. When the fiber tows sinter together at high temperature, the mantle cannot accommodate the rapid dimensional change due to thermal expansion and contraction. This can result in mantle fractures.

While the strength and thermal shock of the mantle can be intrinsically improved by retarding the grain growth by grain boundary pinning, the STTR program funding does not permit an extensive search for suitable chemical constituents, doping or substitute level to improve the mantle shock resistance.

3.2.4 Configuration Factor

The coupling efficiency between the radiation and PV arrays depends on the view factor between them. The ideal geometric view factor is 1, which occurs when an infinite large planar emitter is closely placed in front of a very large planar PV array. The current generator, however, has a cylindrical-shaped mantle and the planar PV arrays are arranged in a hexagonal symmetry surrounding the mantle. The view factor is less than 1. Calculation of the view factor for the generator indicates the coupling efficiency is 26% (**figure 6 of Interim Report, Dec. 1997**)—which means 74% of photons are lost at the top and bottom openings. To reduce this end loss, the opening should be small. This indicates that the generator should adapt a much slimmer cylinder shape. There are limitations, however, on reduction the top and bottom openings by making the PV arrays closer. The distance between the mantle and PV arrays can not be reduced too much. At a closer distance, the exhaust gas envelope will directly impinge on the indium-tin-oxide-coated fused silica filter, resulting in blackbody background. To increase the PV arrays with high aspect ratio also requires even longer mantle — a drawback in terms of mantle initial ignition, combustion uniformity and mechanical strength.

3.2.5 Premixer

a. L-shaped pre-mixer

The first fan-assisted pre-mix delivery system tested is referred to as an L-shaped pre-mixer. This early system consisted of 1" schedule 40 NPT nipples, elbows, tees, and reducers, fitted to form an L-shaped assembly (Figure 3). A highly efficient 24 VDC fan manufactured by Micronel® was placed at one end of the assembly to push air through a mixing tube, while a low pressure (0.5 psi) jet of propane gas was injected using a multiple orifice gas nozzle. To obtain good air-fuel mixing, the gas was injected (placed downstream from the fan) perpendicular to the incoming air. Further mixing was achieved as both gases traveled down the remainder of the assembly (mixing tube) and exited the distributor (port nozzle) into the emitter mantle.

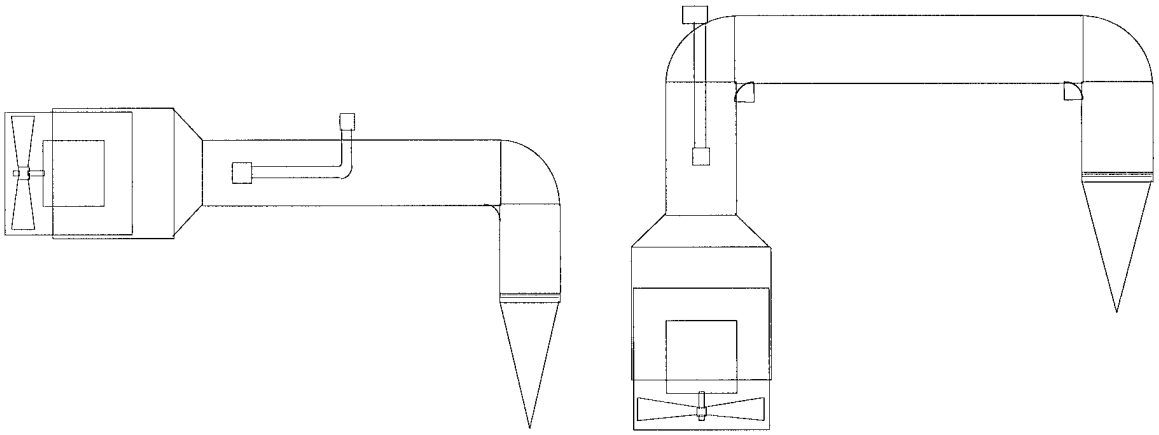

(a) (b)

Figure 3. Conceptual Sketches of (a) L-shaped and (b) U-shaped pre-mixer

L-shaped pre-mixers were tested using ytterbia Oxide (Yb_2O_3) mantles with typical diameters of about 3.2 cm and lengths ranging between 12 and 14 cm. The pre-mixers was tested under gas rates between 8,800 and 14,700 W and burner nozzle back pressures were then measured using Dwyer manometers. Burner back pressures were determined to range from 175 to 300 Pascal which reduced the efficiency of the fan by nearly fifty percent. Another disadvantage of this first pre-mixer was that recuperation was low mostly due to the low thermal properties of the heavy steel walls assembly. Since the distributor was welded to the mixing tube, repairing oxidation damage to the distributor became difficult. The combustion performance, in terms of the flame stability (an indication of a good air-gas mixture) were good. However, this design was susceptible to the combustion by-product build-up during the initial mantle ignition. Therefore, a U-shaped pre-mixer was made.

b. U-shaped Pre-mixers

The U-shaped pre-mixer design considers the mantle pre-ignition mechanics. The advantage of this pre-mixer is much less combustion by-products build-up. Thin-walled brass tube (diameter 3.8 cm) was used to reduce weight and the burner nozzle back pressures, and to increase recuperation capabilities. The premixer gas train was made of a very thin (0.8 mm thick) brass tube. It is light-weight yet sturdy. It has a back pressures of 75 Pascals.

3.2.6 Recuperation

Because the mixing tube and port nozzle are subjected to impingement of hot combustion products and receive radiation from the incandescent mantle, the air-gas mixture passing through the burner components are heated causing these sections and more specifically the port nozzle to act as a *recuperator* where the air-gas mixtures have a higher energy content than before they entered the system. Although recuperation increases the efficiency of the system, a mixture preheated above 550 °C is undesirable, since the temperature of the reactants would favor ignition within the burner and the cracking of the gas. To test the effect of recuperation at the port nozzle, a prototype gas train was assembled and temperatures of the air-gas mixture monitored **Figure** 4. Other variables affecting the mixture temperature were tested including: length of the port nozzle, thermal insulation of the port nozzle, and distributor configuration.

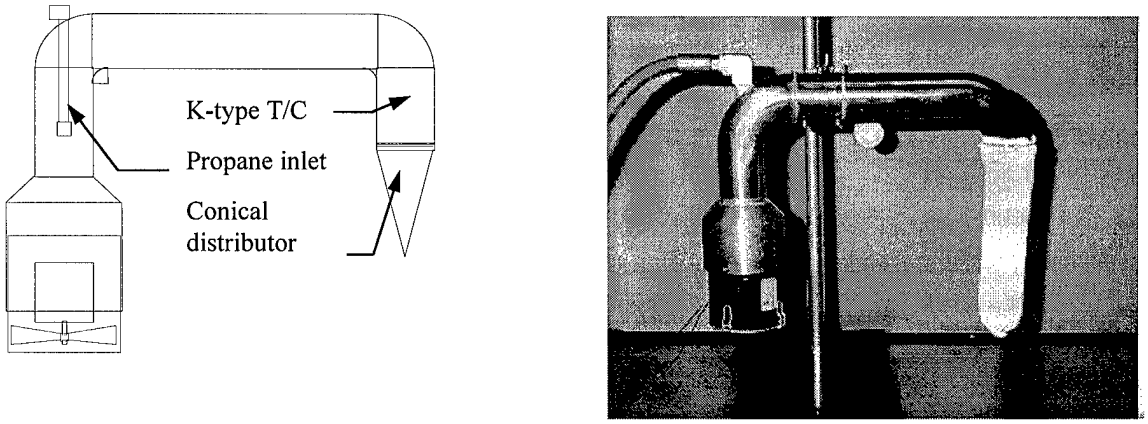

Figure 4 Gas Train Prototype (a) schematic and (b) assembly under test with ytterbium oxide mantle

Table 2 shows the temperature of air/gas mixture measured in the gas train above the distributor due to recuperation. To insure that the air-gas mixture temperature was obtained at the maximum photon output, the mantle was positioned within a quartz cylinder and maximum

photon output was verified with a radiometer located 10 feet away from the light source (IL-1700 and sensor SED-100). Temperatures were monitored with a K-type thermocouple located either in near proximity to the opening of the port nozzle (0.5 cm) or within the distributor cone (1.0 cm). All tests were performed at 11,700 W with the system stabilized for 10 minutes before temperature readings.

The table does not describe all of the tests performed. Some tests did not make it beyond the trial test. For example, a quartz cylinder and a stainless steel cylinder could not be tested further due to immediate flashback, and very poor flame distribution.

Table 2. The air gas mixture temperatures in different distributors due to recuperation effect

Test Conditions (All Tests Performed at 11,700 W)	Air/Gas Mixture Temperature (°C)
Conical Distributor, Port Nozzle Length = 9 cm	576
Conical Distributor, Port Nozzle Length = 5 cm	580
Flat Screen, Port Nozzle Length = 2 cm	205
Flat Screen, Insulated Port Nozzle, Port N. Length = 2 cm	131

3.2.7 Distributor

The fuel and air mixture is injected through the small holes of the conical distributor and burns within the volume enclosed between the distributor and mantle surfaces. The size of the hole in the distributor directly affects the fuel flow resistance, flame distribution, flash-back tendency, and fan back pressure. The fan back-pressure, in turn, delimits the maximum fuel-air mixture possible for TPV generator.

During the component development stage, burner heads of different shapes, including flat screen, perforated cones and perforated cylinders were made and tested. The initial conical design was made of 37 % open area perforated stainless steel (hole diameter of 1.5 mm (0.06 inch)). The base of the cone had a diameter of 3.05 cm (1.2 inch) and the height of 7.6 cm (3 inch). The burner's total surface area was 38.9 cm^2 (actual open area is 14.4 cm^2). The burner flashback at fuel rates below 5,860 W (20,000 BTU/.hr). Thus, the generator has to be run at a higher fuel input rate between 8,800 - 11,700 W (30,000-40,000 BTU/hr), at which 116-124 Watts of gross electrical outputs, can be obtained . To increase the fuel input rate, we examined the possibility of increasing burner area via increasing the height of the burner cone from 7.6 cm to 8..9 cm (3 to 3.5 inches). The total surface area increased to 45.1 cm^2 (open area is 16.7 cm^2). However, this modification reduces gas velocities across the 1.5 mm holes, especially at the tip of the cone, causing frequent flashback and overheating of the tip of the cone. The burner cone generally has a disadvantage of oxidation at the tip and low turn-down ratio. The tip shows oxidation after continuous operation for 10 hours.

To test the maximum heat transfer for the heat sink without destroying the PV array, we needed a burner with a wide turn-down ratio. We used a stainless steel flat screen (53.4 % open area) at

the end of the gas train. We determined the lowest input rate possible for high efficiency. A generator run with the flat screen burner suffers some flame uniformity along the length of the mantle. The cone-shaped burner head improved flame uniformity along the mantle and had lower back pressures (due to the larger open area in comparison to other distributors shape), but it was susceptible to flashback, and it had a short lifetime because of overheating. Very short cones resulted in higher back pressures and non-uniform flame distribution along the mantle's length.

Measurements inside the burner head of conical distributors indicated temperatures close to the fuel's self-ignition temperature of 550°C. Therefore, the length of the burner head was shortened. This resulted in the reduction of the overall surface area which in turn reduced the amount of heat recuperated and the fuel temperature dropped to 400 °C.

Lower fuel input rate has a higher efficiency. Higher fuel input rate has a lower efficiency but a higher power output. The maximum back-pressure for the Micronel® fan, Model 603, set limit to our maximum fuel input to 17,600 W (60,000 BTU/hr).

Since the surface of the burner is exposed to high temperatures, the burner material selection is critical. The material used in the burner head was brass because of its high thermal conductivity and malleability. The flat screen burner never showed problems of oxidation. The cone shape burner, however, suffered severe metal oxidation at the tip. A long tube-shaped burner head made of fused silica was made and tested. The fused silica burner head suffered low pressure drop.

3.2.8 Photocells

Photocell design is also critical for the generator's voltage and power output. The generator requires concentrator photocells due the fact that the radiant intensity at the photocell surface is in the range of 3 to 5 Watts/cm^2—even up to 7 Watts/cm^2 at higher fuel input rate in the generator. The photocells are inter-connected into arrays to cover a large area. The individual photocell's internal resistance and voltage output were matched for efficient combination into sub-arrays. Ten subarrays are connected into an array of 6.7 x 12.1 cm. The ability of the PV manufacturer to fulfill cell and array layout requirements and to deliver a price within the budget limitation was the critical issue for system development.

There are two commercially available silicon concentrator photocells, one from SunPower Corporation (Sunnyvale, CA) and the other from Amonix Corporation (Torrence, CA). The specifications for both SunPower and Amonix cells are given in Table 3. Eventually, the arrays were purchased from Amonix Corporation due to the price consideration and better technical support. While both cells have similar efficiencies, the dimension difference of these cells (1.5 cm vs. 1 cm) altered the number of cells needed in a 6 cm horizontal sub-array from a 4 cells sub-array (for SunPower) to a 5-celled sub-array (Amonix). This changed the voltage output in a sub-array. Individual PV cells mounted on aluminum heat sinks were ordered from Amonix and tested. To avoid overheating, the cells were placed on water-cooled heat exchangers and tested on a mantle premix system. Power outputs obtained from individual cells were compared at a fixed point on the mantle surface. Results indicated 100-200 Watts could be produced using Amonix cells.

Table 3. Cell specification comparison

	SunPower	Amonix
Model:	Model:HDDA 303	AMX-25
Cell Size	1.5 cm x 1.0 cm	1.16 cm x 1.16 cm
Active Area	97% (=1.46 cm^2)	98% (=1.32 cm^2)
Efficiency at 25°C @ 50 suns	24.3%	26.7%
Efficiency at 75°C @ 50 suns	19.4%	22.2%
Availability	limited production run	Shelf item (two junctions)
Max. Concentration	400 suns	250 suns

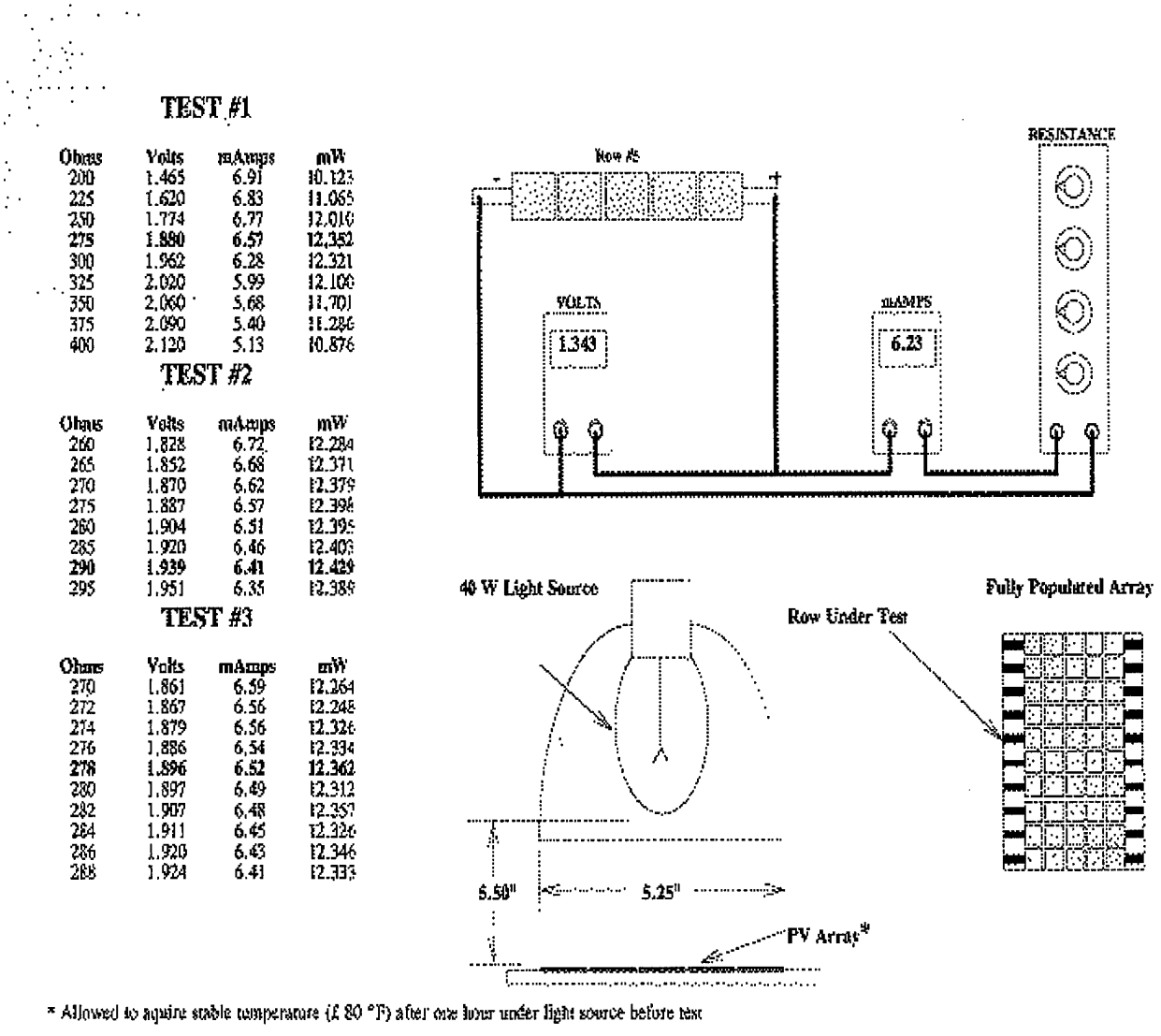

Figure 5. Sub-array under test with a 40W light source.

With encouraging results obtained from these tests, partially-populated arrays (two sub-arrays of 5 cells connected in series) were obtained for characterization of continuity, voltage output, and capacitance. Under a 40 W tungsten light source, the optimal resistance loading of each sub-array was tested to be 232 and 291 Ω. Open circuit voltage, short circuit current and overall internal resistance were tested. The sub-arrays were also characterized, as suggested by NASA, with a capacitance test (dark I-V curve) that shields the arrays from the light completely (Figure 5).

Fully populated arrays, which consist of 10 horizontal subarrays, were also tested in the same way as the sub-arrays. The horizontal subarrays' optimal resistance was 315 ± 39 Ω (268, 274, 281, 284, 297, 327, 330, 356, 363, 370 Ω). Then the array was exposed to a 40W tungsten light source and the open circuit voltage were measured. The V_{oc} result shows less variation than the capacitance measurement.

3.2.9 Array Cooling

For a stand-alone TPV generator, a critical focus is proper cooling of PV cells during operation. Because cooling PV cells drains energy from the TPV itself, it is necessary to have a lightweight, efficient heat exchanger to minimize the power drain.

The heat exchanger design was modeled and implemented by University of Delaware Mechanical Engineering Department using the heat flux data provided by Quantum Group Inc. (Figure 7). A forced-air microchannel cooler design approach, patterned after the work of Kleiner et al. was used as the basis for analysis [Kleiner (1995)].

As described previously in the fifth Quarterly Report (March 31, 1998), the incident flux profile on the PV arrayarrays is of the order of 4 W/cm^2. Excess heat should be removed from the PV (a later analysis found a higher value of up to 7 $Watts/cm^2$). The desired operating temperature of the PV arrays, according to manufacturer's specification, should not exceed 70°C. University of Delaware also minimized the power drawn for fan cooling. The project was carried out in four stages: (1) Preliminary theoretical investigation; (2) In-depth investigation including numerical simulations and characterization; (3) Design and manufacturing; (4) Experimental validation of simulation.

Preliminary analysis showed that natural convection cooling would result in extremely high and hence unacceptable photovoltaic array temperatures. Liquid cooling systems design using components available in the market were found to have low cooling capacity. Furthermore, the U.S. Army was not very enthusiastic about using any liquid for cooling.

Forced convection based on preliminary analysis and from literature offered to be a promising cooling method with both compactness and efficiency. Forced convection could be carried out in two configurations. The first configuration consists of a single large fan supplying air to six heat exchangers. The second configuration consists of six individual small DC fans, one for each heat exchanger. Analysis showed that a single large cooling fan configuration was inefficient compared to the second option. Hence the generator adapted the six individual fans configuration.

980828

TEST No. 107 : Comparison Test of Voc Versus Capacitance
On 3 Pad Amonix Array Used on Test No 82

Setup: (1) Voltage readings (Voc) taken with 40 W light source as shown on page 74.
(2) Capacitance readings taken per setup shown below while cells completelly covered.

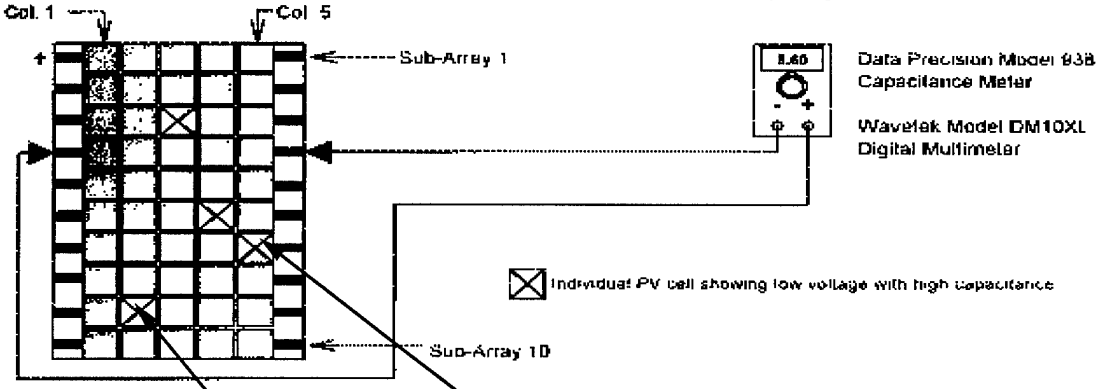

Sub-Array No.	Voc (Volts)	Capacitance (nF)	Column No. / Voc (Volts) of Individual PV Cells 1	2	3	4	5
1	2.87	5.6	0.55-0.58	0.55-0.58	0.55-0.58	0.55-0.58	0.55-0.58
2	2.90	13.6	0.55-0.58	0.55-0.58	0.55-0.58	0.55-0.58	0.55-0.58
3	**2.33**	**74.7**	0.56	0.58	**0.01**	0.57	0.57
4	2.81	13.3	0.55-0.58	0.55-0.58	0.55-0.58	0.55-0.58	0.55-0.58
5	2.88	27.8	0.55-0.58	0.55-0.58	0.55-0.58	0.55-0.58	0.55-0.58
6	**2.33**	**55.5**	0.58	0.56	0.58	**0.01**	0.57
7	**2.30**	**56.5**	0.57	0.55	0.55	0.57	**0.01**
8	2.91	12.3	0.55-0.58	0.55-0.58	0.55-0.58	0.55-0.58	0.55-0.58
9	**2.36**	**89.0**	0.58	**0.01**	0.58	0.57	0.58
10	2.91	2.9	0.55-0.58	0.55-0.58	0.55-0.58	0.55-0.58	0.55-0.58

COMMENTS.

1. A correlation between sub-arrays producing low voltages and high capacitance readings was determined

2. Sub-arrays producing low voltages were determined to contain at least one individual cell producing near zero voltages

Figure 6. Voltage and capacitance measurements of seven PV arrays

3.2.9.1 Numerical Simulation

To design the heat sink for forced air cooling, the heat exchanger's fin pitch, fin height and fin thickness as well as the optimal air flow rate through the heat sink had to be determined. All these factors affect the thermal resistance, airflow pressure drop through the heat sink, power requirement of the fans and power output loss of the PV cell arrays. In addition, thermal

resistance and pressure drop are inversely proportional [Idelchik (1989)]. All this makes the heat sink optimization a complex problem. Hence we carried out the optimization in two stages.

In the first stage we studied various trends of thermal resistance and pressure drop curves for different fin pitches, heights and thicknesses (Figure 8). From these curves, a general working range airflow of 3-5 liter per second and a fin height of 0.75 inch were determined. In addition, we also chose a fin thickness of 0.008 inch. This simplified the search by eliminating three of the unknowns.

Next, a global power optimization on the TPV generator was made. The primary purpose of fan cooling is to reduce the PV cell operating temperature thereby maximizing its output. The power required for the PV cell cooling comes from the TPV generator itself. Earlier modeling (see the fifth Quarterly Report, March 31, 1998) showed as the operating temperature is reduced by increasing cooling fan air flow rate. But we have to pay a heavy price in form of increasing pressure drop, and hence, increasing pumping power. This results in a reduced net power output. On the other hand, if the PV cell is not sufficiently cooled and operates at a higher temperature, a reduced power output from the cell arrays will be experienced. Figure 9 shows PV cell output vs. operating temp decreases linearly. Thus, in the second phase, we optimized the maximum power output as a function of the fin pitch. We assumed that the required power output (that is ,180 W) is produced by the cells at the operating temperature of 50 °C. Considering a particular flow rate, say 4 lps, we see the less power is lost as fin pitch increases, indicating more efficient cooling of a PV with a heat sink of high fin pitch. On the other hand, the pumping power required (a net power loss) to maintain the cell temperature at 50°C also increases with fin pitch more air passage is blocked by the fins.

Graph 1: Heat rejection requirements

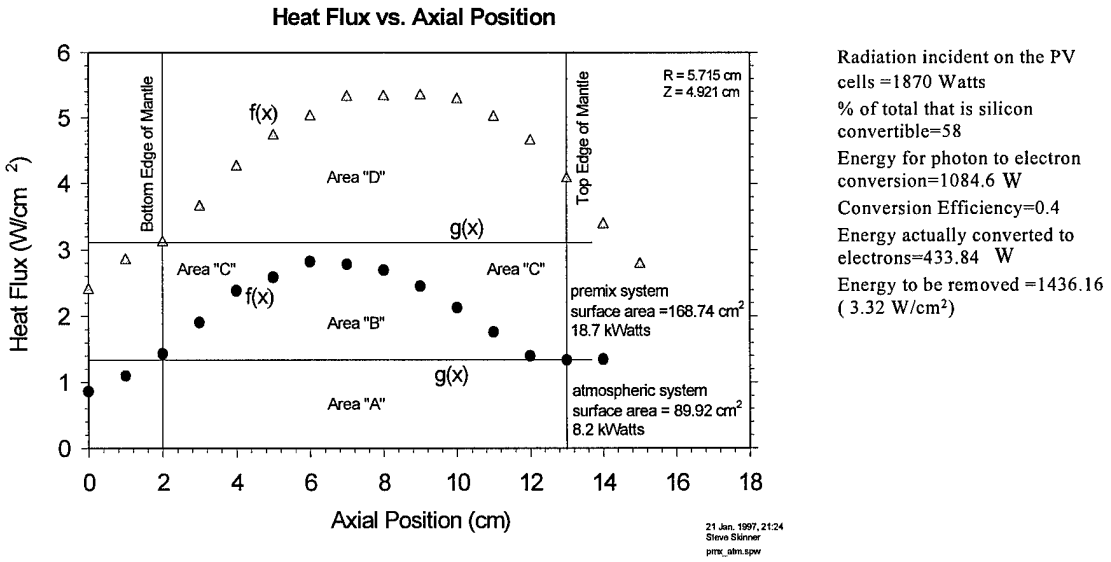

Radiation incident on the PV cells =1870 Watts
% of total that is silicon convertible=58
Energy for photon to electron conversion=1084.6 W
Conversion Efficiency=0.4
Energy actually converted to electrons=433.84 W
Energy to be removed =1436.16 (3.32 W/cm²)

Figure 7. Heat flux measured with a Gorden Gauge for optimization of the heat sink design.

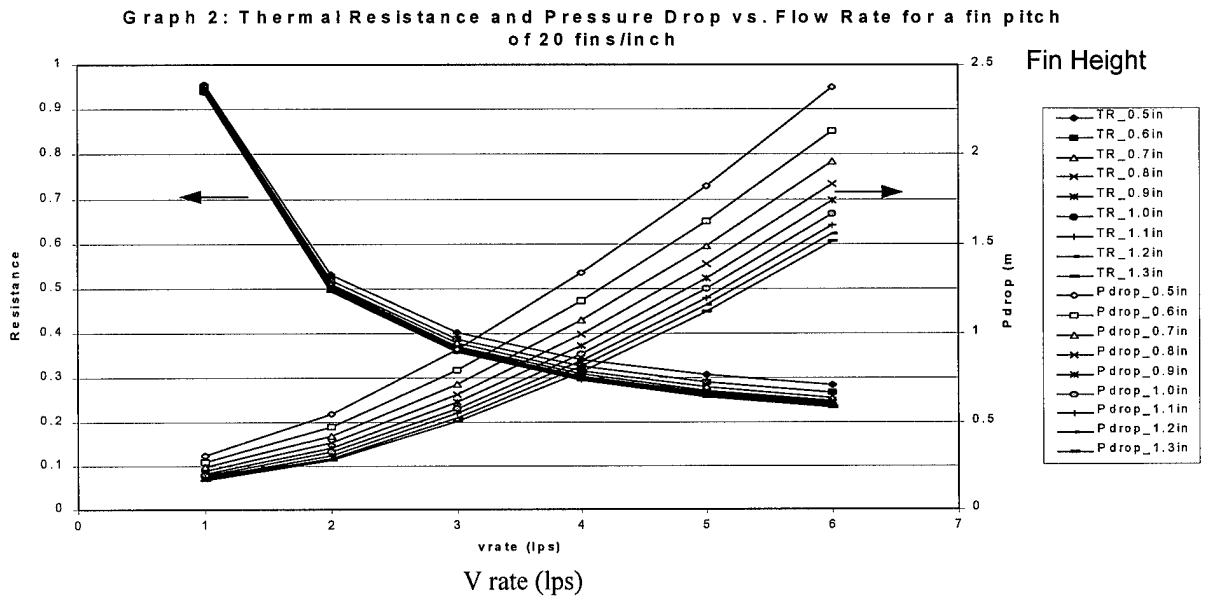

Figure 8. A simulation example of the thermal resistance, pressure drop vs. flow rate for a 20 fin/inch heat sink. Results of different fin pitches, fin heights, fin thickness have been reported in previous Quarterly Reports.

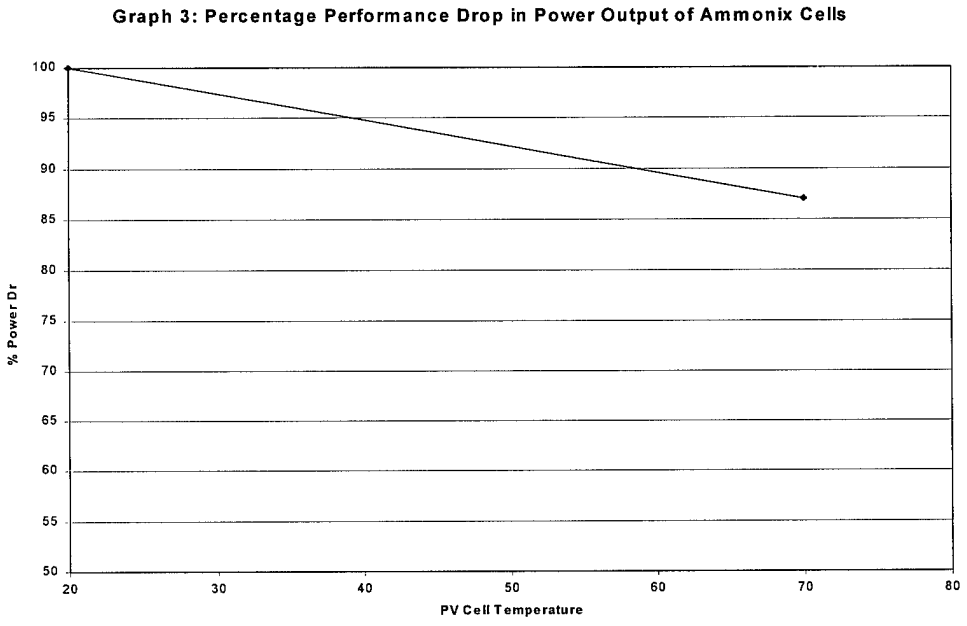

Figure 9. The performance of Amonix cell versus cell temperature

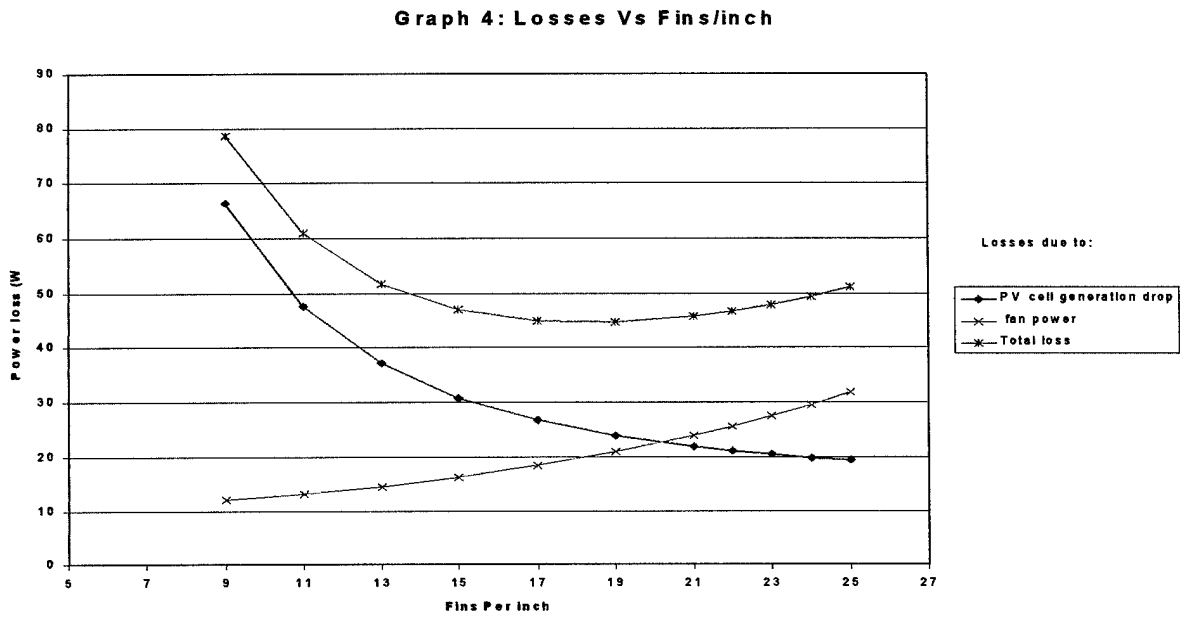

Figure 10. Combined power loss due to the increases in PV cell temperature and cooling fan power (as a function of heat sink fin pitch).

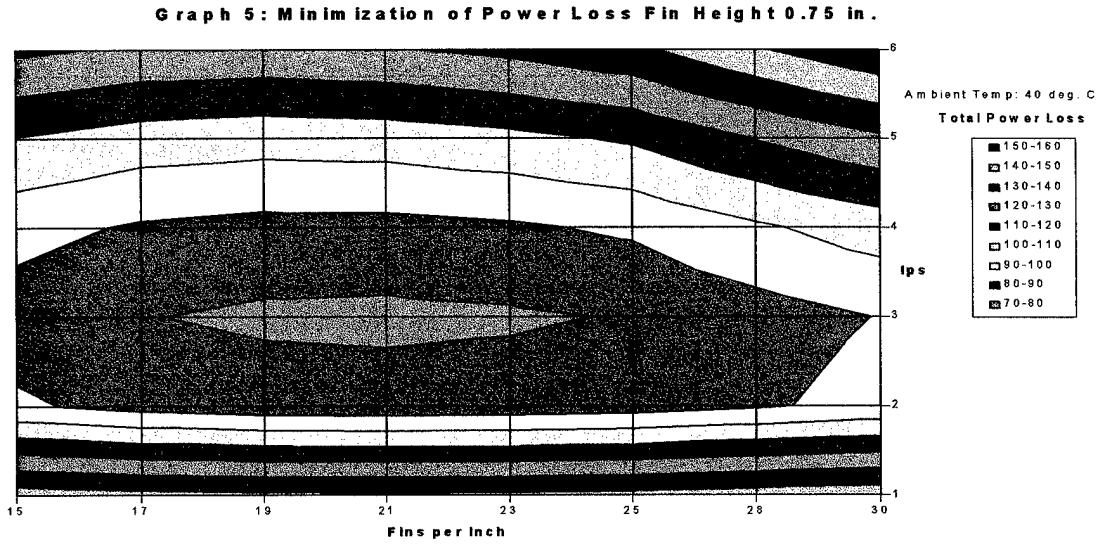

Figure 11. Power loss as a function of fin pitch and air flow rate for a heat sink with a fin height of 0.75 in.)

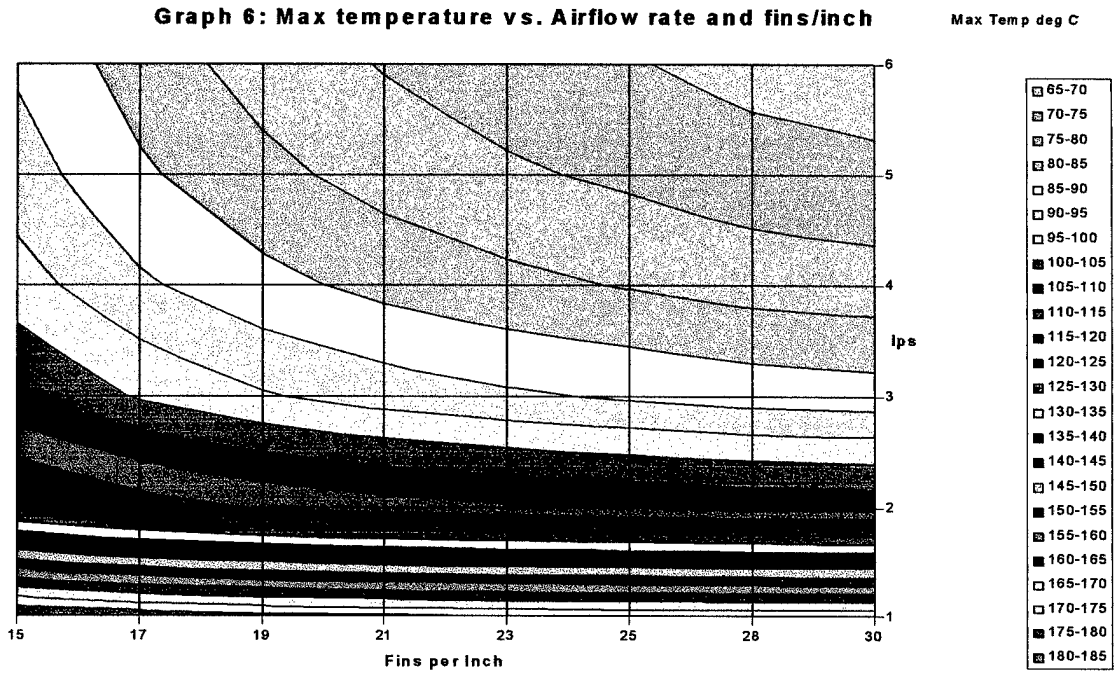

Figure 12. 2-D plot of the maximum TPV temperature vs. flow rate and fin pitch

These two losses are added to get the total losses as a function of fin pitch (plotted on the same graph) The figure shows a heat sink with 17-21 pitch is suitable. Taking this optimization a step further, and considering manufacturing fin height limitation of 0.75 inch, we plotted total losses as a function of fin pitch by varying flow rates from 1 to 6 lps (Figure 11). This graph, which is a 2-D surface contour plot, tells us where the area of minimum power loss lies. We can see the loss has a minimum around a fin pitch of 20 fins/inch. A 2-D plot of the maximum TPV temperature versus flow rate and fin pitch is given in Figure 12

3.2.9.2 Design and Manufacture:

In keeping with the results from the simulation result, we selected the following dimensions for the fins:

Fin type: Plain flat crest
Material thickness: 0.008 inch
Fins per inch: 20 +/- 1
Cut off : 2.38 inch (reference)

Material Type: 1100-0 Aluminum
Fin height: 0.75 inch +/- 0.003
Flow length: 4.73 inch +/- 0.0 1

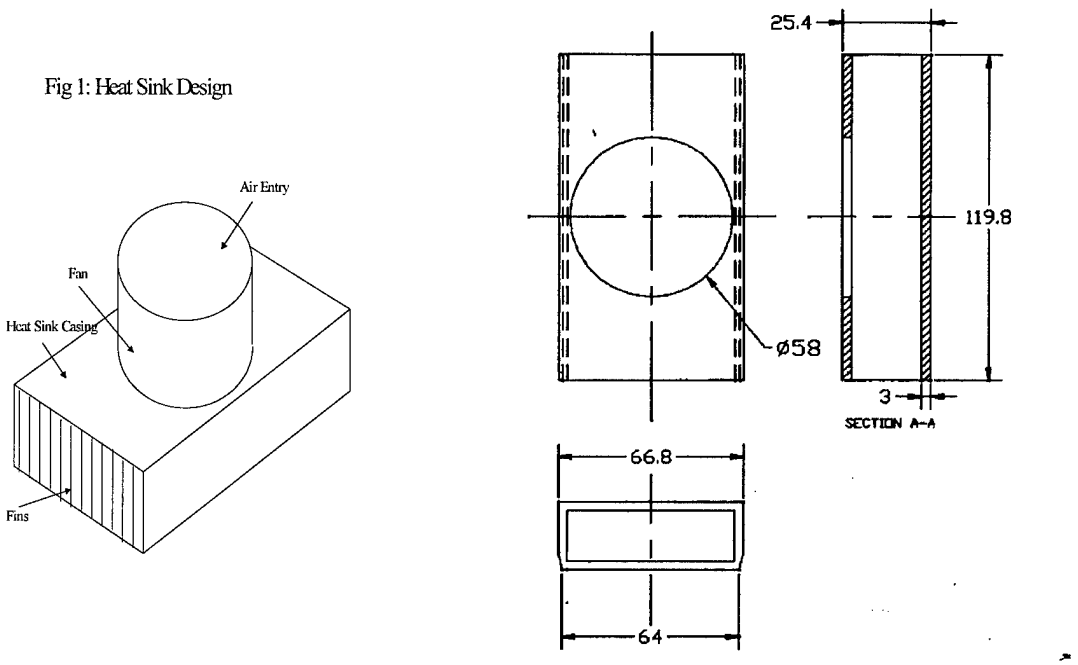

Figure 13. Heat sink design

These fins are to be dip brazed in an aluminum casing. One face of the aluminum case is bonded to the PV Cell array using the thermally conductive epoxy . A fan is to be mounted on the other side at the center of the casing (Figure 13).

The fins would have their top faces cut at center of their length to facilitate passage of air into the heat sink. The fins were manufactured by Robinson Inc and then shipped to Lockhart Industries, where they were brazed to the aluminum casings.

3.2.9.3 Heat Sink Design Validation:

Experiments were performed to validate the simulation results. The thermal resistance was measured using a set-up different from the one used to measure airflow rate and pressure drop.

The set-up for measuring thermal resistance consisted of strip heaters attached to one surface of an aluminum base-plate of the same footprint dimensions as that of the heat sink. No PV array were used in the heat sink design validation measurements. Thermouples were placed in holes drilled parallel and close to the free surface of the aluminum plate. The base plate along with the heaters were embedded in thick Styrofoam insulation. The heat sink was then attached to the free surface of the plate (see figure 22 in Interim Report (Dec. 1997) p..32).

The set-up for measuring the airflow and pressure drop was a fairly simple one. The airflow was measured using a **pivot** tube near the mouth of the heat sink. To measure drop, a small pressure

tap was attached to the wall of a fan near the inlet to the heat sink. This pressure tap was attached by means of a flexible hose to a pressure meter. The experiments conclude:

(1) As expected, temperatures were lower at the center than at the exit. The maximum temperatures measured were lower at 70 °C. (See Figure 14)

(2) The airflow rate was much higher than that expected. This could be because the 90° bend in the airflow channel would not be offering as high a pressure drop as expected. This works to our advantage because we now have more air than expected and hence lower temperatures.

(3) The comparison of thermal resistance shows that the thermal resistance experimentally measured is within 10-15 percent higher than the predicted values. Therefore, the actual maximum plate temperature departs from simulation temperature by 10°C when the heat flux value is higher than 3 W/cm^2. This difference could be due to imperfect thermal contact between the heat sink and the aluminum base plate. Although simulations of thermal resistance differed slightly from the experimentally measured values, the objective of keeping the temperature of the aluminum base plate below 70° C at a heating rate of 4 W/cm^2 was reached (Figure 15).

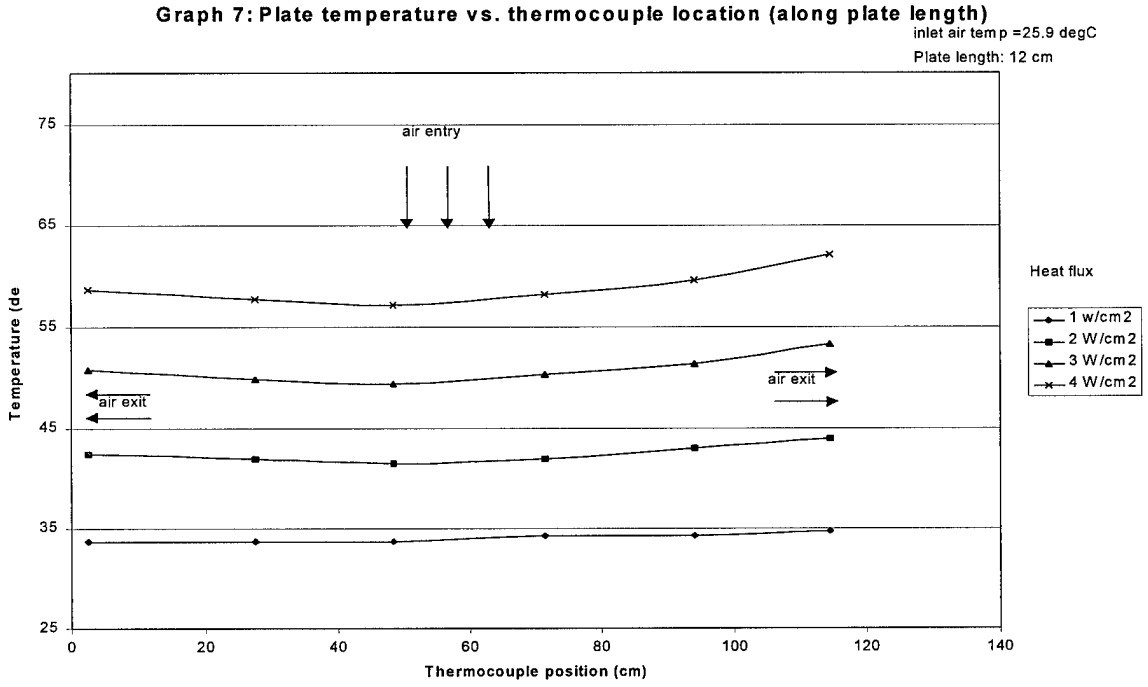

Figure 14. The figure shows the plate temperature versus thermocouple location (along plate length) in heat sink validation experiment. .

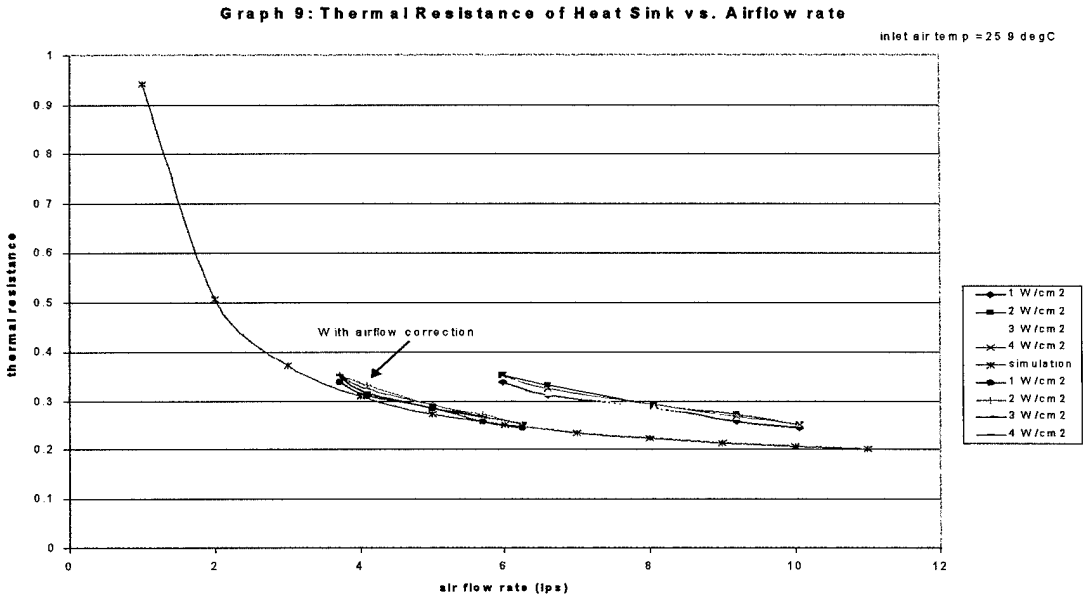

Figure 15. The corrected thermal resistance of heat sink vs. air flow

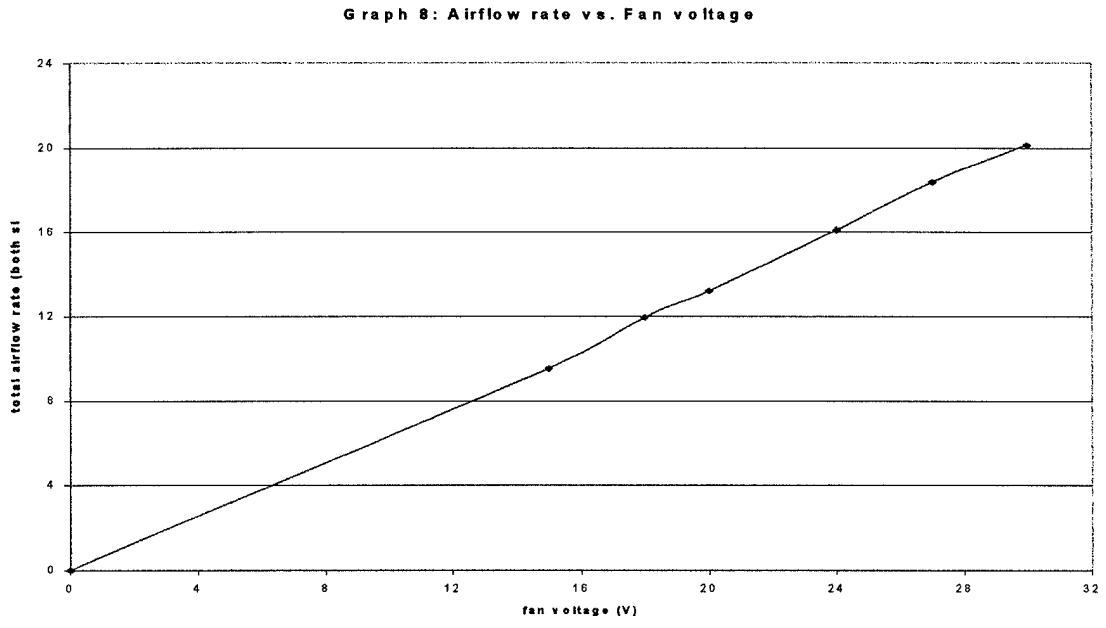

Figure 16. Air flow rate vs. fan voltage for Micronel fan (after 90° bend correction).

Further optimization included fin thickness as an optimization parameter. Figure 16 shows the air flow rate and voltage requirements of the Micronel fan. It requires 12-24 V power to provide sufficient air flow of 8-16 liters per second (both ends) for PV cooling.

4. Prototype TPV generator Fabrication

4.1 Generator Description

The generator consists of a gas bottle, a pressure regulator, a pre-mixer with fan, a manifold, a burner, mantle, an igniter, a fused silica filter. It also contains six photocell arrays, six array heat exchangers, six cooling fans, a hexagonal array interconnection, a DC combiner, a DC-DC converter, three supporting legs, and support structure (figures 17 and 18). The propane fuel, regulated at 0.5 psi., is injected into gas train and mixed with the ambient temperature air. The air is provided by the pre-mixer fan run at 5 Watts of power. The fuel/air is recuperated to 200°C (flat screen port nozzle) before entering the ytterbia mantle.

Burning the mantle for the first time requires the gas train assembly to be lifted up to ignition position outside the generator. The fuel input rate for ignition process, 10,000 BTU/hr. is lower than the operation fuel input rate of 40,000 BTU/hr. After the mantle is burnt, the gas train is lowered to operation position and the fuel input rate is increased to the operation input rate. The power required for the ignitor is provided by a rechargeable 12V/24V battery.

The photons, through an indium-tin-oxide-coated fused silica cylindrical filter, reach the six silicon photocell arrays in a hexagonal arrangement. During the operation, the PV arrays temperature reaches 70-100°C. The PV arrays are cooled by six 24V DC fans, wired in parallel, that consume a total power of 32W. The fan is designed to run by the self-generated TPV power. The six PV arrays are connected in parallel to provide 18V of power output. The DC-DC converter changes the voltage to 24V.

4.2 Prototype Device Architecture and Control Block Diagram

A design of the generator control and function flow diagram is shown in Figure 19. The control flow considers the ignition sequence, safety, over-temperate protection and energy conservation. The fan will stay on for a few minutes to prevent overheating of PV, electronic parts and connections. If, for some reasons, the premix fan fails to operate then the solenoid value will shut off automatically. Not all the control features, however, were installed in the generator prototype at the end of the program.

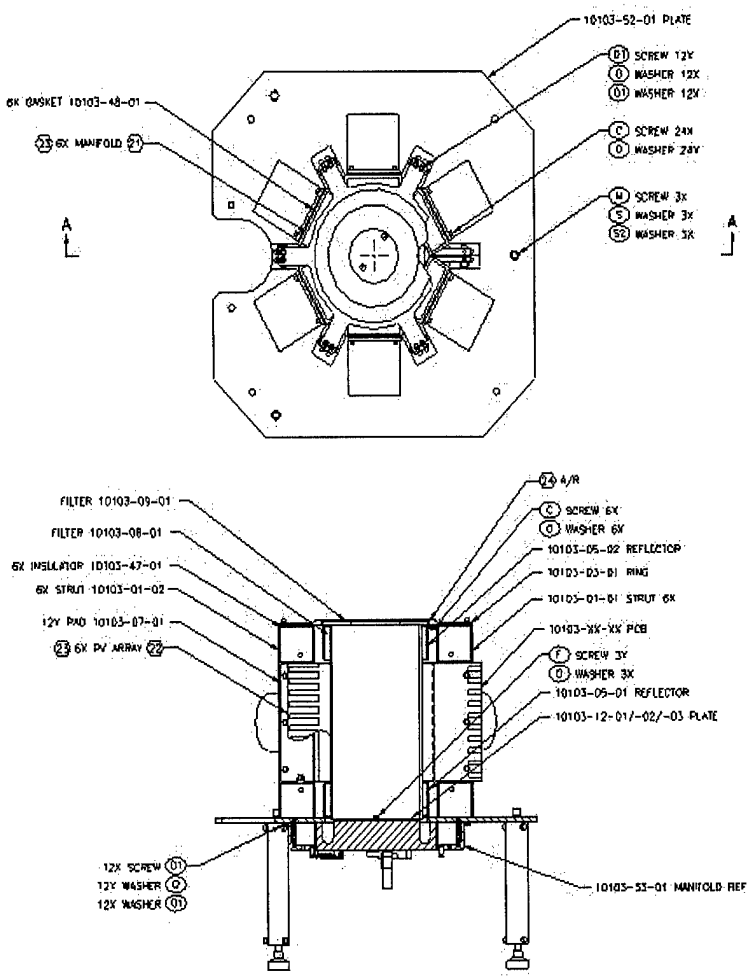

Figure 17. TPV generator design

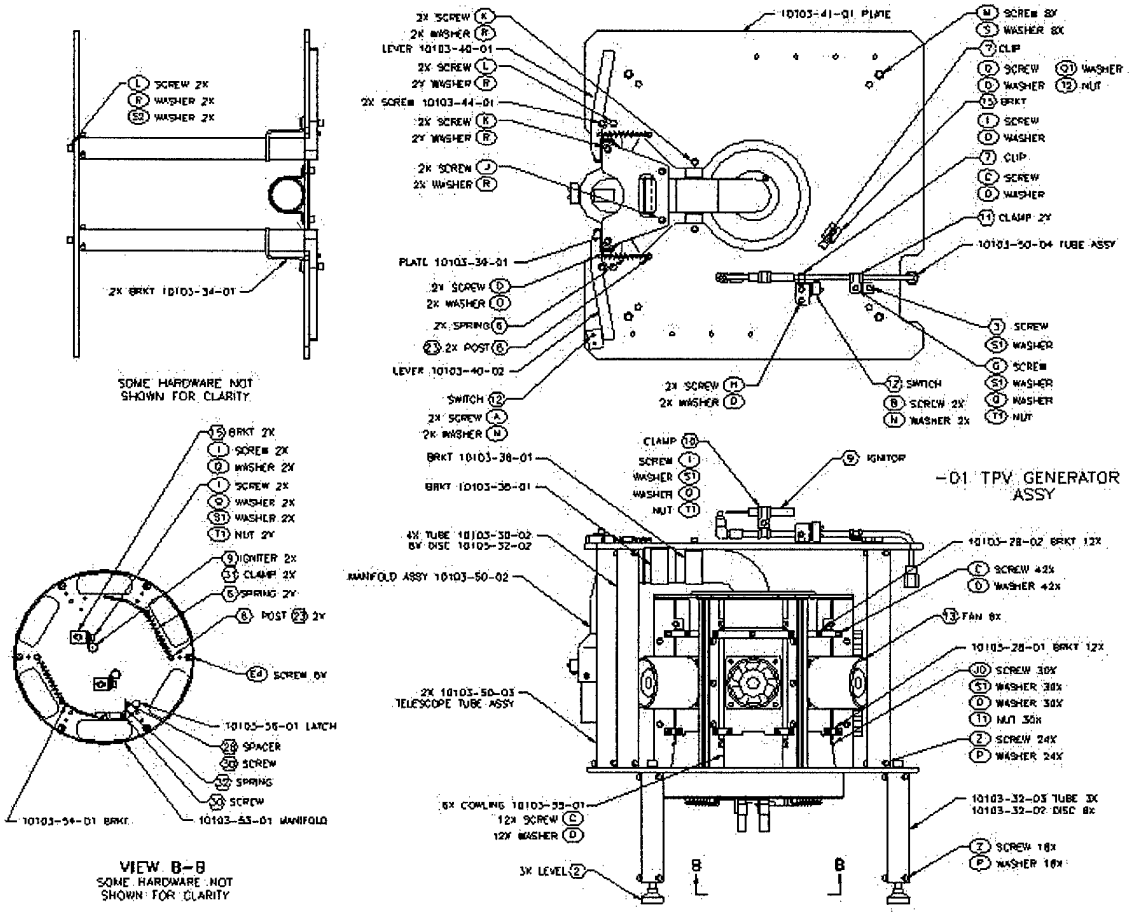

Figure 18. Prototype generator final design (top and side view)

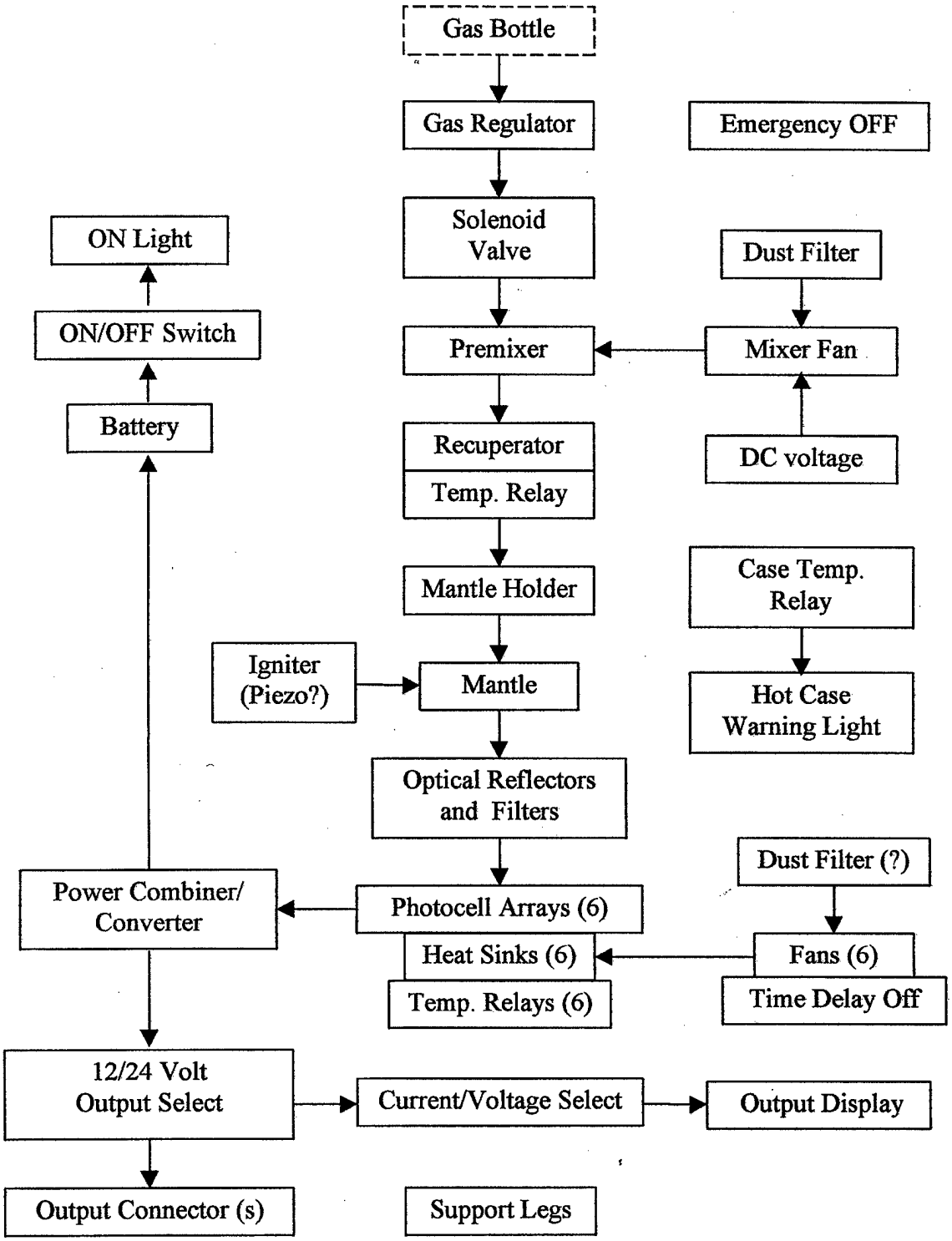

Figure 19. Generator device architecture.

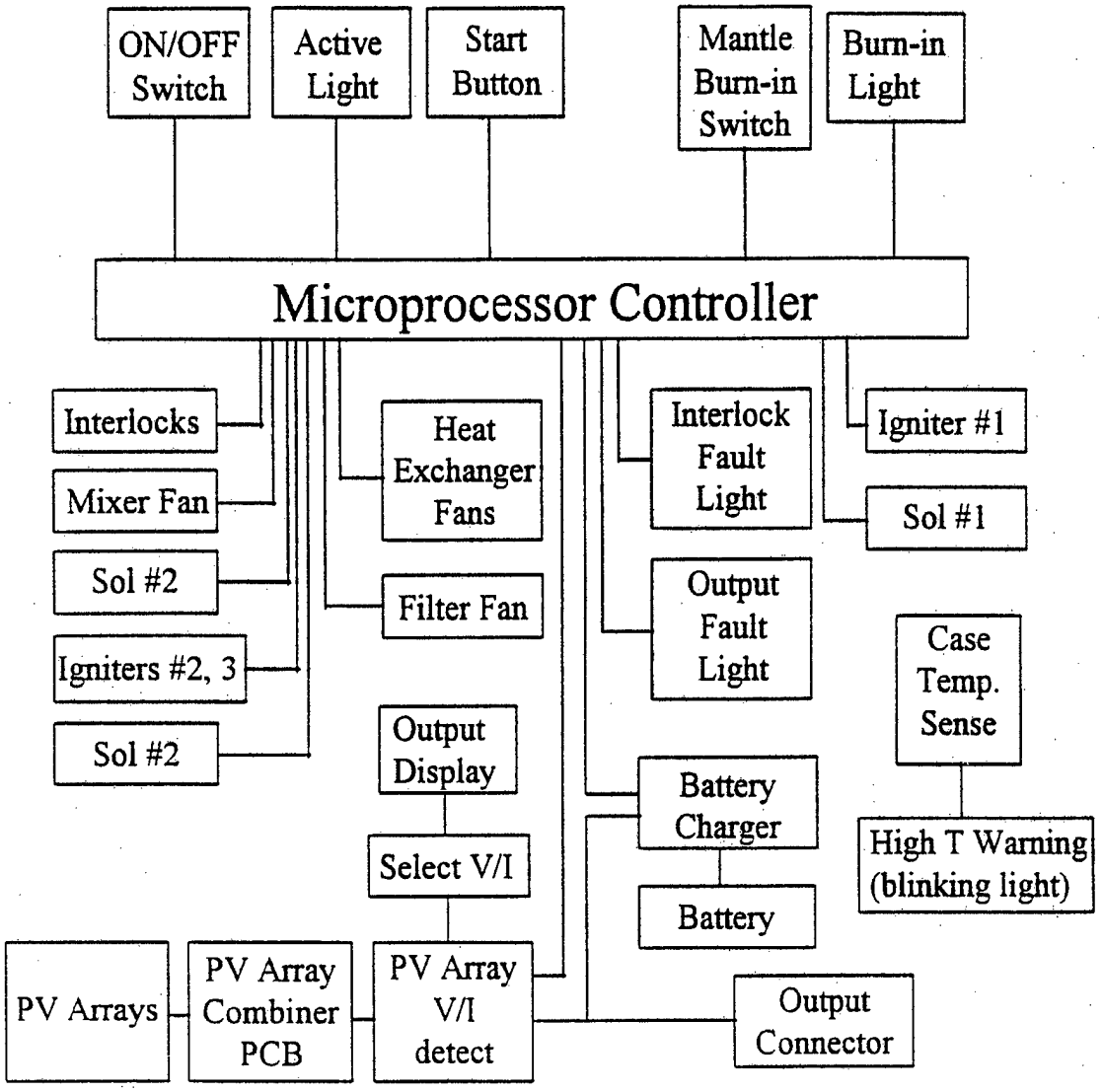

Figure 20. Generator control and display block diagram

4.3 Power Management

An estimation of the power management of the TPV system was made, based on the data collected from component characterization and measurements. As shown in the Selective Emitter Section, a *single* Amonix cell produces 0.67-0.70W when a *double*-layered mantle is operated at 14,600 W (50,000 BTU/hr.). A single cell produces 0.80 W when measured through an ITO-coated fused silica filter. This value was considered the maximum since the measurement was taken with the cell located at the middle section of the mantle, outside the generator assembly. Inside the generator, a conservative estimation of the average power output from a single cell in PV array was 80% of this value due to heating of PV arrays. The power budget of the TPV generator based on single cell data is given in Table 4. One approach for calculation of the TPV generator power budget is from conversion efficiency data. The estimations are shown in Table 5. At each fuel rate, the efficiency and power output were first calculated based on each conversion efficiency process. The numbers shown in parentheses includes the decrease in the fuel to radiant conversion efficiency due to fuel loading . The result in tables 4 and 5 indicate the net power outputs are in the range of 85-125 W for charging batteries.

Table 4. TPV generator power budget based on a single cell measurement

Estimation of Power Budget in TPV Generator from A Single Cell Data	
Single Amonix cell data	
Tested with un-coated fused silica cylindrical filter, 10840 W (37K BTU/hr.)	0.62 W
Tested with ITO-coated fused silica cylindrical filter, 10840 W	0.71 W
Tested with un-coated fused silica cylindrical filter, 14650 W (50K BTU/hr.)	0.74 W
Tested with ITO-coated fused silica cylindrical filter, 14650W	0.84 W
System Output Estimation	
Average percentage output for a single cell in array	80%
Improvement percentage due to end reflectors	15%
Percentage decrease due to PV cell temperature increase	13%
Total power generated ($300 \times 0.84 \times 0.8 \times 1.15 \times 0.87$)	202 W
DC to DC conversion efficiency 90%	182 W
Power Used by fans (preliminary estimation)	56 W
Projected net power output	125 W

Table 5. Estimation of power output based on conversion efficiencies .

	Efficiencies of Conversion Processes						
	$Q_{fuel} \Rightarrow V_f \times Q_{rad}$ =11%, Measured @ 18700W		Measured and Calculated	Calculated	Measured		Fan power 35 W
	Estimated	Calc.					Meas.
Fuel Rate (W)	$Q_{fuel} \Rightarrow Q_{rad}$ 42%	V_f × 26%	$Q_{rad} \Rightarrow Q_{Si\text{-}band}$ × 58%	$Q_{in\text{-}band} \Rightarrow Q_{PV}$ × 18%	$Q_{DC\text{-}DC}$ × 90%	Efficiency (%)	Net Power (W)
8790	3692 (3635)	960 (945)	557 (548)	100 (99)	90 (89)	1.0 (1.0)	55 (54)
11700	4910 (4510)	1280 (1172)	740 (680)	135 (122)	120 (110)	1.0 (0.9)	85 (75)
15000	6300 (4910)	1640 (1278)	950 (741)	170 (133)	154 (120)	1.0 (0.8)	119 (85)

1. The system efficiency = $(Q_{rad}/Q_{fuel}) \times V_f \times (Q_{Si\text{-}band}/Q_{rad}) \times (Q_{PV}/Q_{in\text{-}band}) \times (Q_{DC\text{-}DC}/Q_{PV})$
2. Values inside parentheses accounted for mantle fuel loading effect
3. All conversion efficiencies measured outside of the generator
4. Efficiency $Q_{in\text{-}band} \Rightarrow Q_{PV}$ is based on cell temperature at 100°C
5. No reflectors effect is accounted for this estimation

4.4. Hardware Development

4.4.1 Gas Train and Distributor Testing

The gas train and distributor were manufactured in-house at Quantum Group, Inc.. As stated previously (**Distributor Section**), we have tested different lengths of the conical burners and a flat burner. We re-tested these burner heads in the generator in order to observe flame distribution, flash back tendency and fan pressure. The generator was run at 11,700 W (30,000-40,000 BTU/hr), to obtain the required 120 Watts gross electrical output. The burner cone generally has a disadvantage of oxidation at the tip and low turn-down ratio. The tip shows oxidation after continuous operation for 10 hours. This led us to change the distributor to a flat screen type- that has a better turn down ratio. The flat screen burner, however, suffers some flame non-uniformity along the length of the mantle. The input rates were adjusted for the possibility for high efficiency and for high power output. As stated previously, the maximum fan back-pressure limits our maximum fuel input to 17,600 W (60,000 BTU/hr). The operation fuel rate is, therefore, between 11700-14650W (40,000-50,000 BTU/hr).

The major advantage of the U-shaped pre-mixers is less accumulation of combustion by-products and has a similar fan back pressure as the L-shaped mixing tube. Therefore, the U-shaped pre-mixer was used in most of the generator performance tests. Several design modifications have

been made to see whether improvement can be made in the axial heat flux distribution and installation of the mantles. A screw-on type distributor was designed to fit to the pre-mixer but was not able to be manufactured in time for testing. Cylindrical metal and fused silica distributors were also fabricated. Cylindrical distributors, however, showed poor axial heat flux distribution and were quickly disregarded due to the program time limitation.

Temperature measurement near the distributor indicated that recuperation was responsible for 40 % of the radiant fraction conversion as the air-fuel mixture reached 380 to 450 °C. It may be possible to increase recuperation temperature if a burner head is installed to obtain a super-heated mixture. The final configuration used at the distributor was a plain screen placed within the nozzle adapter. The screen was made of stainless steel with a 53.4 % open area. It had a port loading between 2,800 and 3,500 W/cm^2, and could be operated at very low input rates (1,500 W or less) without flashback. By comparison, a conical distributor allowed port loading of only 523 to 890 W/cm^2 for equivalent input rates (8,800 - 15,000 W).

4.4.2 Spectral Filtering

The optical filter is an important part of the TPV design. An ideal optical filter only passes the narrow band that matches to absorption spectrum of PV cell, thus, reduces heat rejection requirements for PV cells and increases overall system efficiency. It also prevents the combustion flue gas from reaching PV arrays by conduction and contamination from the combustion by-products. The reflected energy is assumed to be recuperated. In reality, some unwanted energy is also transmitted through the filter. Some energy is absorbed and re-radiated by the filter.

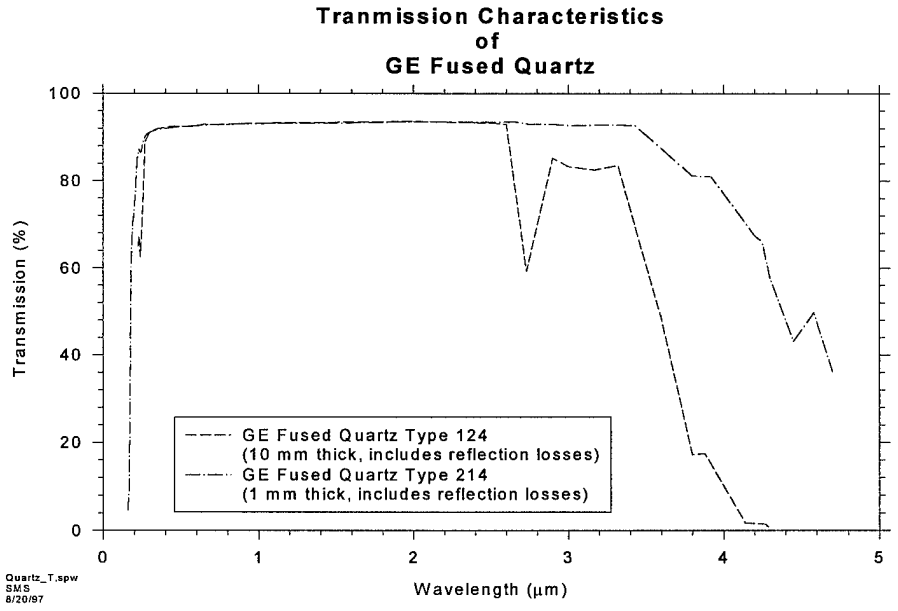

Figure 21. Transmission Characteristics of General Electric Fused Quartz

Our selection of ITO-coated fused silica cylindrical filter is based on available literature. W. E. Horne describes an indium-tin-oxide (ITO) filter and shows that the long wavelength absorption is about 20% and in-band transmission is about 75% [Horne (1996)]. Similar results have been reported by S. D. Murthy [Murthy (1996)]. The drawback of the filter is that it reduces the ruggedness of the generator and increases cost.

Commercially available optical glasses such as Schott GG495 or Schott F2 may be suitable as the filter. Both are transparent at 1,000 nm range (transmittance of about 92 - 98%) and have cutoff near 2,500 nm. However, given the requirements for spectral range, operating temperature, thermal transient and gradient, fused silica is still a good material. The long wavelength cutoff of quartz is about 2.7 micrometers, with a some transmission beyond that. Figure 21 shows typical transmission characteristics for "wet" and "dry" fused quartz Spectral improvement can be accomplished with a thin film coating of indium-tin-oxide. The transmission, reflection and absorption characteristics of this material are shown in Figure 22 [Baldasaro (1994)].

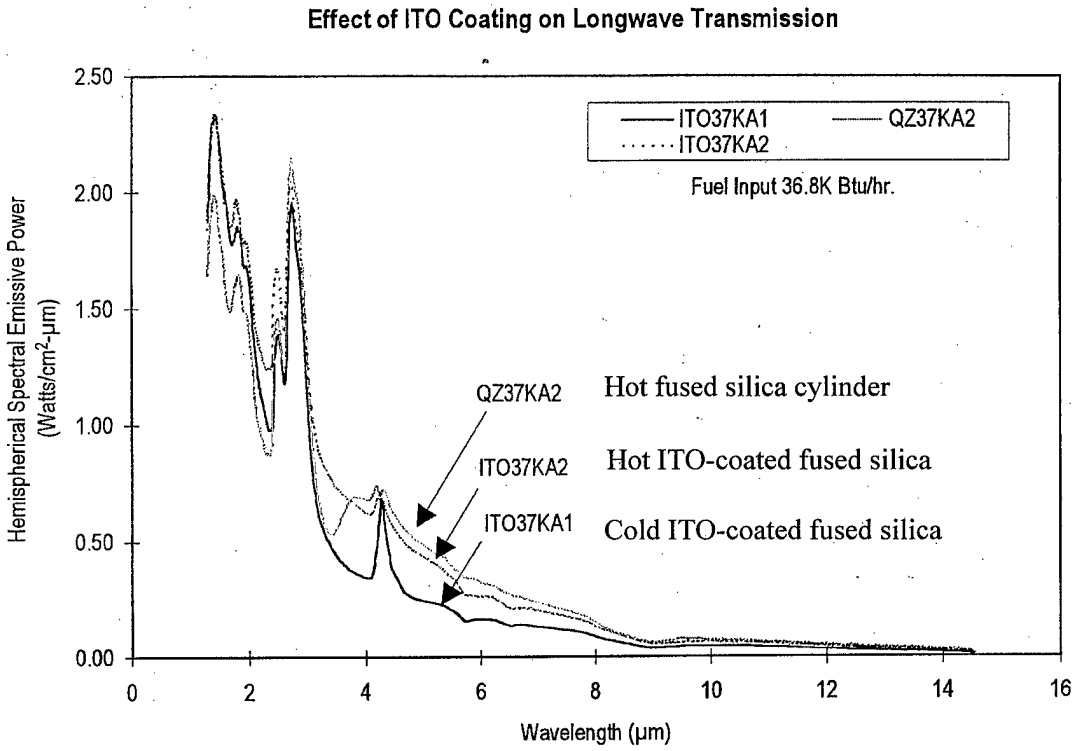

Figure 22. The transmission spectrum of ITO-coated fused silica. Fused silica has the highest long wavelength transmission. ITO-coating, however, is effective in cut-off beyond 3 μm (ITO37KA1) when cold but less effective when hot after heated up for more than 5 minutes (ITO37KA2).

4.4.3 Bonding the PV Arrays to the Heat Exchangers

a. Adhesive Selection

Initial preliminary tests were performed using soda-lime glass pieces cut to emulate the final dimensions of the photovoltaic arrays (6.7 cm x 12.1 cm). The two best candidates were determined to be a tack free adhesive (AI Technology, Inc.) and an aluminum filled epoxy (Cast-Coat, Inc). Both showed good electrical and physical properties (Table 6.).

The aluminum epoxy must be used in a semi-liquid form, the tack free film adhesive must be applied in the same manner as a label. A series of preliminary tests were performed with glass plates to see which compound was better. Glass pieces are good for observing trapped air bubble formation and irregularities in the adhesive between the plates. Bubbles within the components are undesirable since they will increase the thermal resistance between the surfaces in contact, as will a layer that is too thick. A combination of glass pieces and aluminum plates were later used. The aluminum plate was used to test flow characteristics and to examine problems related to the application of the film or semi-liquid epoxy. Finally, plates made of 1100 aluminum were machined to dimension specifications, including thickness and flatness. The thickness of the adhesive was targeted to be 0.006 inch.

Table 6. Physical and Electrical Properties Comparison of a Dielectric Film, and of Dielectric Epoxy Compound.

AIT EPOXY FILM ADHESIVE		CAST-COAT DIELECTRIC COATING	
Electrical Resistivity cm	< $4x10^{-4}$ ohm-	Specific Gravity: @ 25°C	179
(160 °C/ 10 min)		Viscosity: cps, uncatalyzed @ 75°C	6,500 -7000
Dielectric Strength (Volts/mil)	Not	cps, catalyzed @ 30°C	6,500 - 7000
Applicable		Thermal Conductivity: Btu/ft^2-hr-°F/in	31.5
Glass Transition Temp.(°C)	-60	Tensile Strength: psi @ 23°C	8,900
Current Carrying Capabilities	>200A/mm^2	Compressive Strength: psi @ 25°C	18,500
Lap-Shear Strength	>1000 psi	izo Impact: ft. Lbs / in of notch	0.49
	>6.9 N/mm^2	Coeff. of Thermal Expansion, in/in/°C x 10^{-6}	28
Device Push-off Strength	1500 psi	Heat Distortion: °C	65
	10.3 N/mm^2	Water Absorption: 7 days @ 25°C, %	0.1
Hardness (Shore A)	82	Linear Shrinkage: in/in	0.003
Cured Density (gm/cc)	3.5	Service Temperature: °C, continuous	-70 to 95
Thermal Conductivity	45 Btu-in/hr-	Standard Color	
ft^2-°F		Aluminum	
	6.4 W/m-°C		
Linear Thermal Expansion Coeff. (ppm/°C)	110		
Max. Continuous Op. Temp. (°C)	150		

The pre-mixed semi-liquid epoxy and hardener were warmed at 50 °C to reduce viscosity and facilitate air bubble removal. Stubborn small bubbles were removed by applying a vacuum of 20-30 in. Hg for 1 minute on 50-gram batches. For the dielectric film, the glass plates with a pre-cut piece of the film were pre-heated to 80 °C for a few minutes. When the plates acquired the same temperature, a second plate (pre-heated to same temperature) was then placed over the first plate.

The result indicated aluminum-filled epoxy was less problematic. With careful practice and trials, several successful bubble-free sets of plates were produced. Although a pre-formed adhesive film was simple to apply, its application was more difficult than anticipated — the film had always folded on itself increasing the thickness of the overall assembly. Joining the plates required trial and error of various techniques.

b. Joining of the PV Arrays to Finned Heat Exchangers

The semi-liquid aluminum-filled epoxy was prepared in 50-gram batches, following the manufacturers procedures. Upon applying the epoxy compound, the assembly was then allowed to dry for 48 hours at room temperature. A standard method to join the plate was established and two of the successful assemblies were then sent to UoD for thermal performance analysis.

4.4.4 Array interconnection

The combination of jumpers and connectors is designed to allow any interconnecting scheme in series and parallel of the 10 rows of PV sub-arrays and produce 30 or 15 VDC. The vertical wires can be chosen randomly for series connections between arrays. By placing jumpers in the right locations, a desired output combination can be achieved. The 30 VDC is good for a 24 VDC regulated power battery charger. The 15 VDC can be employed to obtain a 12 VDC regulated power supply. The 30 VDC, for example, is obtained using pairs of arrays connected as the following and shown in the wide tracks connection schematic in Figure 23:

Connecting Scheme	Jumpers between
Row 10 in series with row 1, In parallel with:	I37-6 and I38-6; I40-5 and I39-5: I1-5 and I2-5; I4-6 and I3-6
Row 9 in series with row 2, In parallel with:	I33-6 and I34-6; I36-4 and I35-5: I5-4 and I6-4; I8-6 and I7-6
Row 8 in series with row 3, In parallel with:	I29-6 and I30-6; I31-3 and I32-3: I9-3 and I10-3; I12-6 and I11-6
Row 7 in series with row 4, In parallel with:	I25-6 and I26-6; I27-2 and I28-2: I13-2 and I14-2; I16-6 and I15-6
Row 6 in series with row 5,	I21-6 and I22-6; I23-1 and I24-1: I17-1 and I18-1; I19-6 and I20-6

4.5 System Integration and Testing

Most of the problems encountered in the integration of the generator were associated with mechanical design and thermal management, or a combination of both.

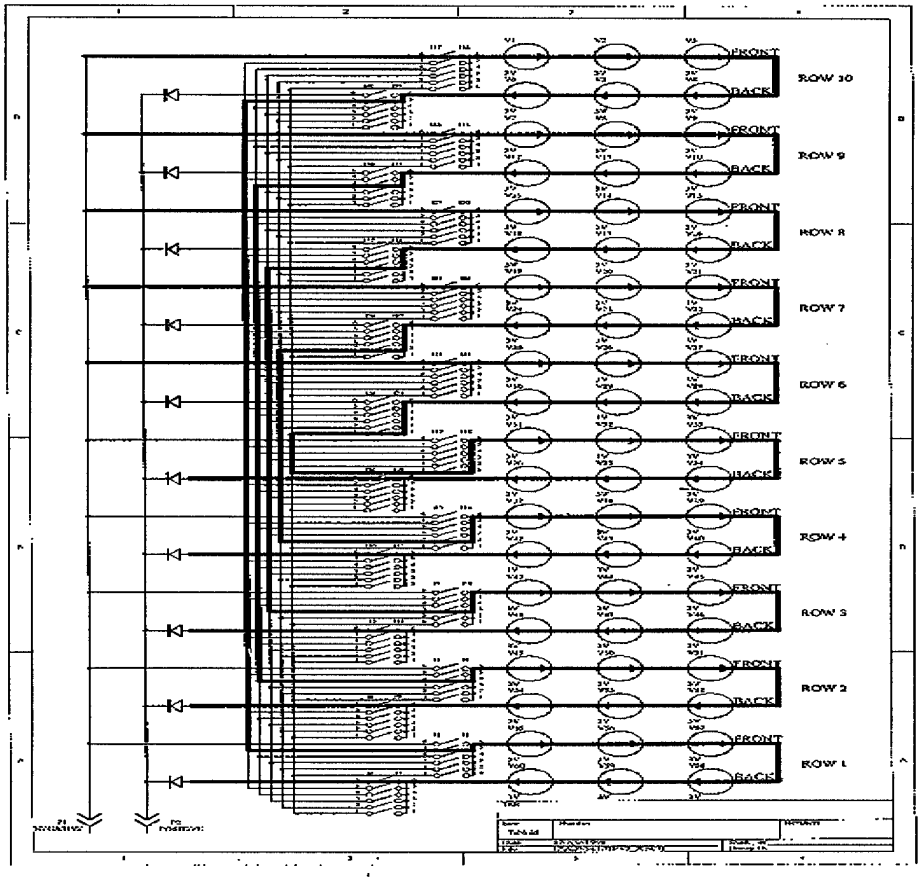

Figure 23. The wide tracks show the connection schematic for 30 VDC.

4.5.1 Air Flow Test and Modification

As the generator operates, the six PV arrays located 4.5 cm away become hot. Cool air is drawn into each of the heat exchangers by a dedicated high efficiency fan located on the back of each the heat exchanger. The hot air exits through the top and bottom of the six heat exchangers (Figure 24).

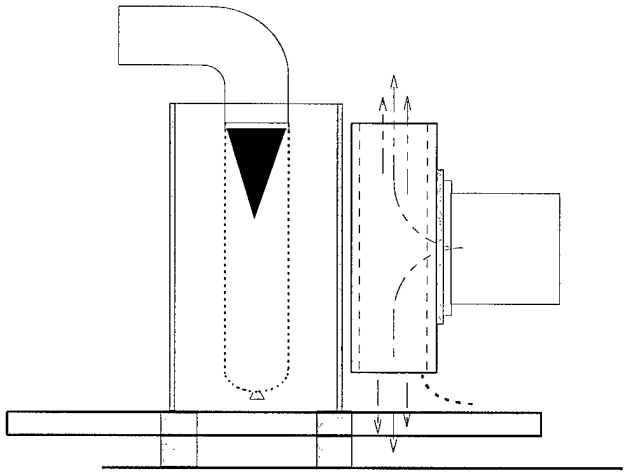

Figure 24. Schematic Drawing Showing Airflow Pattern Within Heat Exchanger

Tests were conducted to determine airflow pattern in the generator using a device that produced a visible smoke plume near the fan. The results indicated that the air exited through the bottom of the heat exchangers was deflected by the plate serving as the base for the PV arrays. Some of the deflected air was recycled by the fans that supposed to provide only the fresh air for the cooling of the arrays. The distance between the heat exchangers and the surface on which the arrays rested was increased in order to minimize the recycling effect of the heated air. However, because of the self-imposed maximum height limitation, the distance between the heat exchangers and the base plate can only be increased by a few centimeters. To verify the efficacy of this modification, tests were performed at a fuel input rate of 8,800 Watts. Thermocouples were instaled on the fan housings to monitor the temperature. The result indicated that when the incoming air was isolated from recycling (placing a long conical cowling at the intake), the temperatures dropped by an average of 20°C (from 50 °C to 30 °C), indicating recycling still existed.

To remedy this condition, the bottom plate was modified by machining rectangular openings in the base plate at the bottom exits of the heat exchangers. This would allow the hot air to go through without deflection and thus could prevent recycling. This time, however, the bottom plate got much hotter (than before the openings were made). The failure was thought to be due in part to the large mass of aluminum that the plate was made of (1.3 cm x 37 cm x 37 cm).

The hexagonal PV arrangement has an open area of about 250 cm^2 below mantle, therefore, it was necessary to place a reflector there (In comparison, the PV area exposed to the mantle emissions is 432 cm^2). With this in mind, a system of aluminum ducts mounted on a cowling surrounding the base of the generator was conceived to act as air ducts to cool the bottom reflector. Part of the flow was diverted through these ducts to cool the ITO-coated fused silica filter. The mass of the plate was also reduced by reduce the plate thickness from 1.2 cm to 0.6 cm. This modification reduced the mass of the plate by 50%. The reflector was also placed in thermal contact with the new cowling and a support plate allowing the absorbed heat to dissipate much faster. This attempt, however, failed to prevent the air recycling. The temperature of the reflector increased to failure point (see **End Reflectors** section).

In the final design, the cowling at the base of the generator was removed and was replaced by a parabolic reflector. With the parabolic reflector, thinner aluminum plate and square holes, average temperatures on the fan housings was maintained at 32 °C at 8,800 - 11700 Watts of fuel input rates (Figure 25).

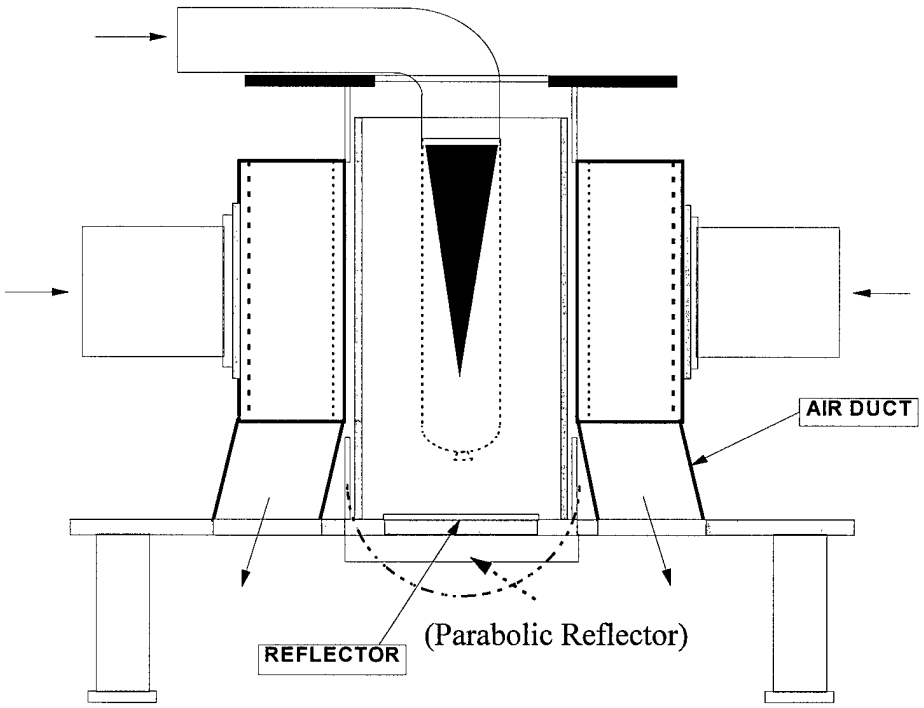

Figure 25. Base plate showing openings for air escape path. Flat reflectors are also shown.

The fan that cools the heat exchanger has a maximum operating temperature of 65 °C (Model D603M-24VDC, manufactured by Micronel®). When the system was operated at rates of 11,700 W, the temperature limit was again reached. Because of this, gaskets made of alumina fibers were used to reduce the conduction heat. Afterward, temperature dropped to 35 to 39 °C.

4.5.2 End Reflectors

The initial generator design had a bottom reflector plate that attached with a 24 VDC fan (12 cm x 12 cm footprint). The fan was designed to provide forced-cooling air between the fused silica cylindrical filter and the PV arrays. To provide cooling to the quartz cylinder, a 24 VDC fan Model KDB241238LB6A manufactured by Elina Fan was placed under the photovoltaic array beneath the bottom reflector (Figure 26).

The bottom reflector was a gold-plated metal disc made of high-temperature alloy. Three gold-plated metal (Kanthal™) flat discs of 8, 10, and 12 cm in diameter were tested as end reflectors. These discs divided different amounts of air between the fused silica cylinder and the PV arrays

(Figure 25). The first two discs were thermally isolated from the metal base by a ceramic fiber insulator felt (Fiberfrax™).

In the first test, the 8 cm diameter disc turned red-hot and became badly distorted after 5 minutes of continuous firing at 8,800 Watts of fuel rate. A second gold-plated metal disc was tested under an ITO-coated quartz disc. This disc also distorted by the intense heat. In both cases, the gold coating became non-reflective after the tests. A third gold-plated disc was placed in direct thermal contact (metal to metal) over a modified base plate to reduce the heat load. The gold plating, however, did not survive at the end of the test. Temperature readings obtained with the system running at up to 15,000 W were too high (above 500 °C), so it was decided to redesign the base plate to allow the use of gaskets or in a different scenario and remove the fan all together. The cooling fan design was then changed to a parabolic reflector design.

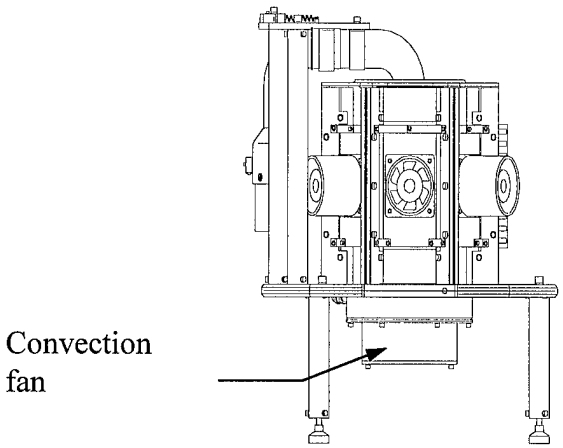

Figure 26. Drawing Showing the Proposed Location for a Convective Fan.

A parabolic reflector, made of aluminum, was used as the bottom reflector (dash line in Figure 25). It has a dimensions of roughly 15.5 cm in diameter and 6.0 cm deep. The wall thickness is 1.1 millimeter. Two parabolic reflectors with two diameters (15.5 cm diameter and 12.0 cm diameter) were tested to check their influence on the output of the system. Both produced identical results and held well through the tests. **(NOTE**: The parabolic reflectors were obtained from a radiant heater manufacturer. They were designed to reflect light but not directed to the PV arrays. The reflectors had their centers perforated —undesirable for the generator since the mantle-cylinder system focused light at the center of the generator's base. However, these reflectors are light weight, inexpensive and improved system performance.)

The top reflector design was a gold-coated fused silica toroid or a stainless steel holder to hold the gold-coated quartz toroid. Both designs were never implemented due to late delivery of parts. A re-design of the bottom reflector to divert light to the arrays (instead towards the mantle) should improve the light uniformity. It will be beneficial to have a high-temperature IR coatings (gold + SiO_2 for example) and solid surfaces (that is, no perforations).

4.5.3 Assembly of the PV arrays

Because of the hexagonal configuration of the photovoltaic array assembly, two photovoltaic electrical leads from each array were sandwiched to form contact. However, bending stress occurred through slight mechanical misalignment or thermal expansion and resulted in array detachment from the heat exchanger. The bending forces acting on the arrays were later removed by anchoring the struts to the heat exchanger with thin brackets, thus removed the stress from the array.

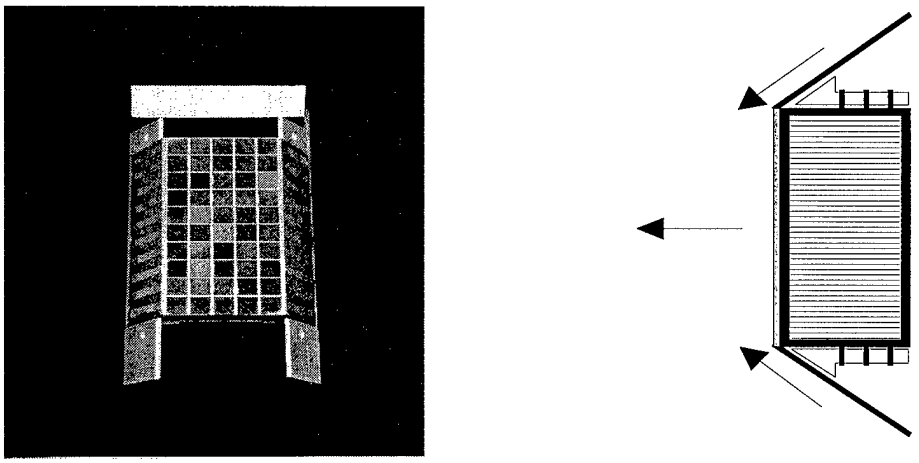

(a) (b)

Figure 27. (a) Photo of hexagonal photovoltaic array assembly showing thin brackets for support(b) bending forces acting on array while heat exchanger fixed in position by screws.

4.5.4 Ignitor, DC-DC Converter and Display

A mini-ignitor made by Norton Company (24 VDC @1.7A) was used to ignite the generator. Preliminary tests showed successful ignition regardless of the ignitor's locations either at the top or at the bottom of the fused silica cylinder. The ignition can also be done with a sealed end or an air gap at the base of the fused silica cylinder. The top location is, however, better for the initial mantle ignition.

A small, standard DC-DC converter (International Power Devices) was used to convert the voltage to a regulated 24 VDC. The conversion efficiency is 85-90%. The conversion efficiency is nearly independent from 50% to 100% of generator output. As described in Quarterly Report (June 30 1998), the loaded output voltage of six sub-arrays, connected in series, is between 15-18 VDC. Generator load varies due to the charge characteristics of batteries, which draw less current as they near fully-charge.

The system has a voltage and an amperage meter for power monitoring. The final design is lack of a self-diagnostic display.

4.6 Prototype Operation and Performance

The extended legs were removed from the original generator for better stability during usage (Figure 28). In its final configuration (Figure 29), the generator is a self-contained, self-powered system. It produces a gross power up to 122 Watts and a net power of 85 Watts to recharge batteries. Dimensionally, the generator could be referred as a portable or a mobile system (with an overall height of 45 cm and a footprint of 37 × 37 cm and its final weight just 9.0 Kg)

The process to ignite the mantle was still left as a manual process to be performed in two steps. The reason for this choice is related to the emitter (mantle), which consists of a delicate ytterbia oxide mantle similar to the one used in camping lanterns. The great advantage of using these mantles is that large numbers of them can be carried by the soldier without special requirements for storage. Two manual processes are required in order to set the generator in motion: 1) Loading or attachment of the mantle to the port nozzle, and 2) Lowering of the mantle within the photovoltaic cavity before initiating ignition. This process was chosen at this time because allows verification of the physical condition of the mantle prior to the use of the generator. Only one mantle should be used for one battery charging period. While the mantle's time-to-failure is yet to be defined, there was enough indication that the operation limit may be longer than 10 to 12 hours. The system needs little after-use power consumption for cooling since the overall temperatures drop to about 30 °C within 3 to 5 minutes after shut-down.

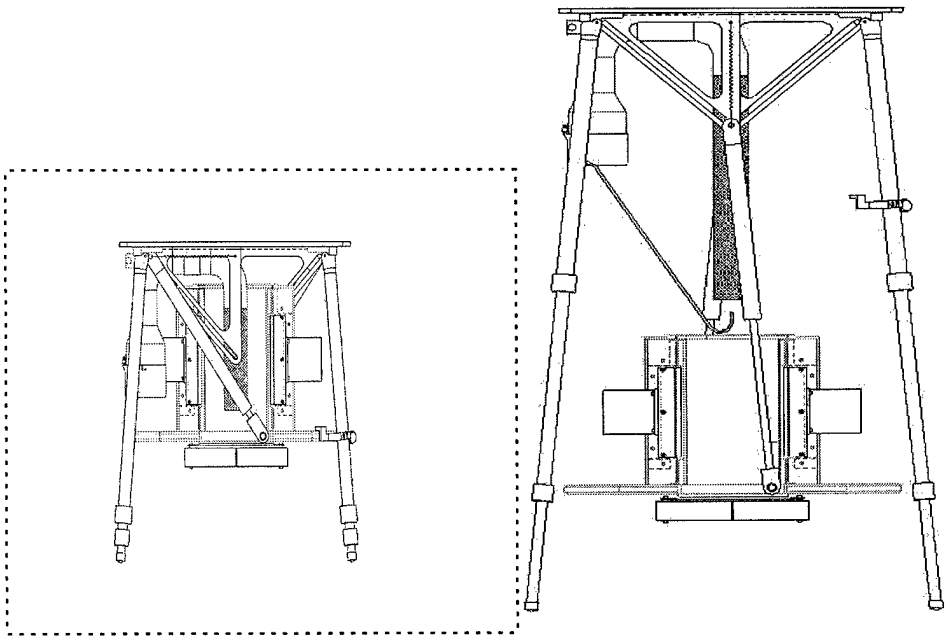

Figure 28. The original generator design has an extended legs for initial mantle ignition

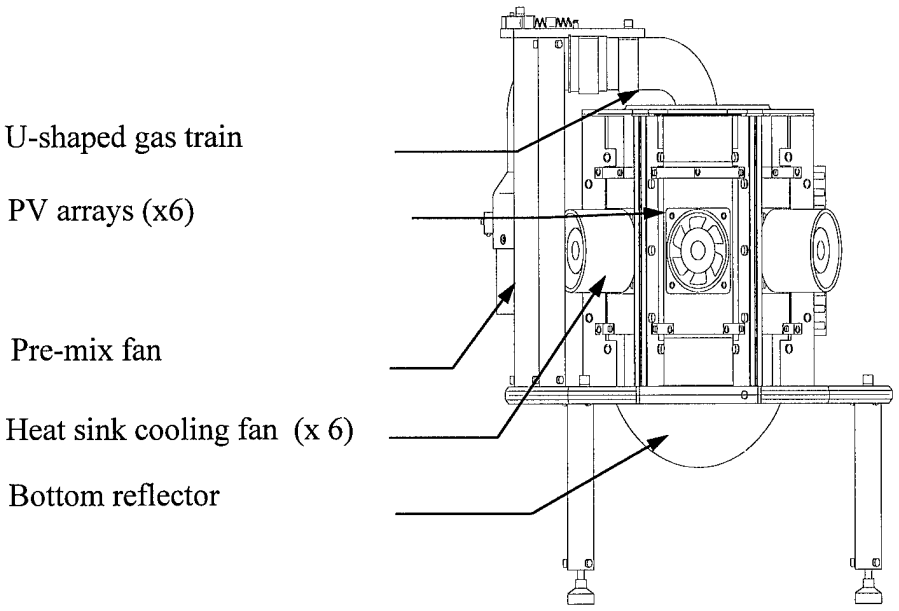

Figure 29. The final prototype TPV generator design removed the extended legs for better stability

The achievements of the project were also reflected the generator's low profile and weight, but also in its ability to continuously operate with a single mantle. The prototype generator produces 122 W of electric power at a voltage of 24 V and a current of 5 Amperes. The system's overall fuel to electric power conversion efficiency is 1%. The generator requires six Mcronel® fans to cool PV arrays and an additional cooling fan for premixer. The total power consumption is 37 Watts, leaving only 85 Watts of net power. The main shortfall in efficiency is due to large end radiation loss in cylindrical geometry and slight over temperature of PV cell than the designed value. This end loss can be improved with the better end reflectors directed to the PV arrays.

At the operation burning rate of 40,000 BTU/hr (117,23 W), a 9.07 Kg propane tank (5 gallon) can run continuously for 10 hours and charge 5 batteries.

5 Conclusions

The TPV portable generator developed in this effort demonstrated the integrated system performance of a compact generator design within the requisite space envelope of less than two cubic feet delivering 122 watts of electricity with 37 watts to run cooling and combustion air pre-mixer fans. Therefore, net power output of 85 watts is available for charging batteries. Key components of the TPV generator demonstrated in this effort include:

- a fuel delivery system with a TPV powered electrical fan to provide the forced air for combustion,
- a relatively large 1.5 inch diameter by 8 inch long ytterbia selective emitter to convert fuel energy to selective photons,
- six TPV cell arrays with a total of 300 silicon semiconductor cells to convert selective photons to electricity,
- forced air cooled TPV cell arrays with six TPV powered electrical fans for cooling each individual array to reduce TPV cell array dark current losses which improve semiconductor efficiency,
- an electrical voltage controller to interconnect multiple TPV cell arrays into the desired voltage outputs,
- an internal cylindrical shroud to protect the TPV cells from combustion gases and
- effective methods of reducing system weight and reflecting photons back to the selective emitter.

This generator is entirely self-powered and only needs a portable gaseous hydrocarbon fuel supply, such as propane, to provide the combustion energy. For this task, the generator was constructed primarily for stationary operation in a vertical orientation. Also, each time the generator is refueled the mantle should be replaced to ensure durable and efficient operation.

From the experience of this effort, Quantum Group is positioned to build four prototypes of the present generator for Army field test with an up front effort to complete the nine incremental performance improvement tasks defined by Quantum Group in our Phase III STTR proposal dated August 1,1998. These prototypes would weigh about 15 lbs. and operate at 1% efficiency.

If a step change in configuration and materials with higher performance are desired, then significant improvements can be realized in the next version of this generator. However, only one prototype unit will be delivered for this situation. Key performance parameters, and how to improve them, are given below:

- **Efficiency**
  Improve Combustion System Recuperation and also the View Factor between emitter and TPV cell arrays.

  This task requires a major change in geometry for both the emitter and the fuel delivery system. Although the present cylindrical system did demonstrate some recuperation, this geometry had a poor view factor and will need to be modified to provide a closer coupling from the emitter to the cells and to heat incoming combustion air. It is expected that a flat

plate, or a radiant tube burner with selective and transparent materials, or a light pipe, or an evanescent coupled light pipe with smaller sub modules will give a better optical view factor. For future development work, Quantum Group is positioned to deploy both optical analyses and straightforward fundamental tests on several small-scale innovative concepts described under a pending provisional patent to improve the efficiency.

- **Orientation Independence**
  Change the fuel delivery and mantle construction and topography to provide other passages for combustion gases to escape while at the same time improving the view factor.

  Since forced air is already provided to the incoming combustion air, the fuel delivery system can be readily modified to work under all orientations. However, since a large portion of the losses are due to poor conversion of combustion fuel energy to radiant photon energy, more work is needed to reduce the heat lost via combustion products. As an example, radiant tube burners have been reported with good orientation independence and high efficiencies - these burners coupled with a low cost and efficient spectral selective emitters control method could improve overall performance.

- **Durability**
  Develop stronger emitter structures.

  The large size and high temperature mantle currently employed in the present TPV generator represents a significant advance. However, a more robust mantle can be developed with Quantum Group's new emitter technology concepts. Some approaches include bonding selective emitters to transparent high temperature materials that provide higher mechanical strength, smaller modular mantles, and spherical high energy density emitters. A modular design approach with modest size repeatable modules that can be arranged to give the desired electrical output should be pursued. Alternate concepts should be pursued at a modest research cost to include tasks such as high temperature selective emitters bonded to transparent light pipes, optical interference and plasma filters for reflecting low energy photons back to the source, more efficient optical emitter to TPV cell array geometry (e.g., flat plates, spheres, or selective emitter light pipes). Successful development will lead to a long life mantle configuration and improved mechanical shock performance.

- **Affordability**
  Develop affordable TPV semiconductor materials and fabrication processes.

  The approach in this TPV generator with available silicon semiconductors and spectral control via ytterbia selective emitters has potential to be a low cost approach. Even with these lower cost semiconductors and emitters, today's costs are prohibitive for large-scale deployment of TPV at 100 watts. The expected cost of various alternates including various silicon architectures, different semiconductor bandgaps and emitter materials, high voltage multi-junction cells, and concentrator cells should be evaluated. An economic study based on today's technology forecast is needed to set the manufacturing direction on semiconductor architecture.

6. Bibliography

1. Baldasaro, P.F. Brown, E. J., Depoy, D. M. , Campell, B.C. et. al., and Parrington J.R., "Experimental Assessment of Low Temperature Voltaic Energy Conversion,' First NREL Conference on Thermophotovoltaic Generation of Electricity, *AIP Conference Proceedings 321* (1995) pp.29-36.
2. Horne, W. E., Morgan, M. D., and Sundaram V. S., "IR Filters for TPV Converter Modules," The second NREL Conference on Thermophotovoltaic Generation of Electricity, *AIP Conference Proceedings 358* (1996) pp.35-41.
3. Idelchik, I. E. and Fried E., "Flow Resistance, A Design Guide for Engineers," Hemisphere Publishing Corporation, 1989.
4. Kleiner, M., B et al., "High Performance Forced Air Cooling Scheme Employing Microchannel Heat Exchangers" *IEEE Transactions on Components, Packaging, and Manufacturing Technology*, vol. 18, No. 4, pp. 795-804, Dec 1995
5. Murthy, S. D. et. al., "Characteristics of Indium Oxide Plasma Filters Deposited by Atmospheric Pressure CVD," ibid. pp. 290-311.